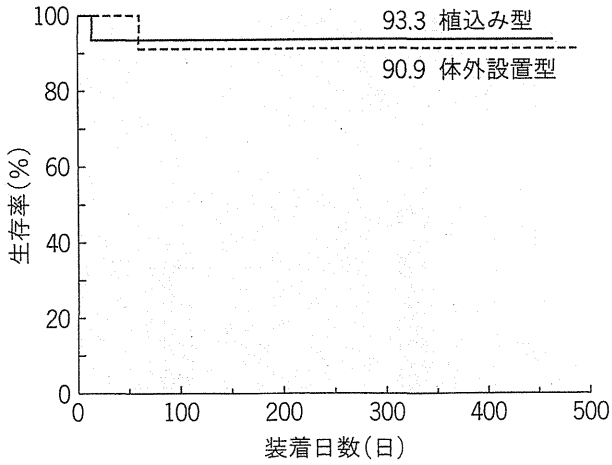

図4. 当センターにおけるLVAS装着例の生存率

INR）のリバースを行うことにより，症状の重篤化の防止に努める．当センターにおいては，2009年以降の体外設置型LVASにおける2年生存率は88%と，良好な成績を示している．

また2011年4月からは，植込み型LVASが心臓移植へのブリッジ例に対する適応として保険償還された．このため2011年4月以降は，植込み型を第一選択としてきた．これまでに植込み型LVAS 16例，体外設置型11例に装着を行ってきたが，死亡例はそれぞれ1例で，植込み型は脳血管障害，体外設置型は感染症であった．1年生存率はそれぞれ93%，91%と良好な成績を示している（図4）．特に植込み型では在宅管理を行うこととし，VAS外来を設けている．また最近認可されたコアグチェック（エーザイ社，東京）を用い，PT-INR管理を行うようにしている．

Ⅲ．心臓移植およびLVASの今後

わが国における心臓移植の成績は良好であり，2011年より植込み型LVASが心臓移植へのブリッジとして保険償還された．このため長期の待機を行う場合においても，植込み型LVAS装着により在宅での待機が可能となった．心臓移植および植込み型LVASによる末期心不全に対する治療選択として，広く受け入れられるようになってきたことから，心臓移植およびLVAS治療を行う体制整備が求められている．

当センターでは，2001年に重症心不全・移植病棟を開設するとともに，医師，看護師のみならず，レシピエント移植コーディネーター，人工心臓管理技術認定士，メディカルソーシャルワーカー，薬剤師，理学療法士，臨床工学技士，栄養士，栄養サポートチーム，感染制御チーム，精神科などのチームを作成し，心臓移植対象および移植後患者に対応する体制としてきた．今後このようなチームが，多くの医療施設で構築されることが望まれる．

おわりに

1）末期心不全に対してわが国においても心臓移植および補助人工心臓が治療選択として受け入れられるようになり，その施行数も増加し，その成績は良好である．

2）心臓移植の適応年齢は，60歳未満が望ましいから65歳未満が望ましいに変更されることになっており，また新たな植込み型補助人工心臓が心臓移植へのブリッジとして保険償還されようとしており，今後わが国での末期心不全に対する心臓移植および補助人工心臓を組み入れた治療体系の整備が必要である。

文　献

1）Stehlik J, Edward LB, Kucheryavaya AY et al：The registry of the International Society for Heart and Lung Transplantation；29th official adult heart transplantation report. J Heart Lung Transplant **30**：1052-1064, 2012
2）日本心臓移植研究会：本邦心臓移植登録報告（2011年）．移植 **45**：537-540, 2011
3）Nakatani T：Heart transplantation. Circ J **73** [Suppl A]：A55-A60, 2009
4）中谷武嗣，藤田知之：わが国における臓器移植の現状と今後―心臓移植．医のあゆみ **237**：397-403, 2011
5）Fujita T, Toda K, Nakatani T et al：Risk factors for post-transplant low output syndrome. Eur J Cardiothorac Surg **42**：551-556, 2012
6）Kitamura S, Nakatani T, Bando K et al：Modification of bicaval anastomosis technique for orthotopic heart transplantation. Ann Thorac Surg **72**：1405-1406, 2001
7）Wada K, Takada M, Nakatani T et al：Limited sampling strategy for mycophenolic acid in Japanese heart transplant recipients；comparison of cyclosporin and tacrolimus treatment.

Circ J **71**：1022-1028, 2007
8）中谷武嗣，簗瀬正伸，村田欣洋ほか：わが国における心臓移植でのエベロリムスの現状．今日の移植 **22**：674-678, 2009
9）簗瀬正伸，中谷武嗣：心臓移植交代関連拒絶反応の診断と治療．心臓 **42**：20-25, 2010

SUMMARY

Heart Transplantation and Ventricular Assit Systems

Takeshi Nakatani, Department of Transplantation, National Cerebral and Cardiovascular Center Hospital, Suita, Japan

Hiroki Hata, Tomoyuki Fujita, Junjiro Kobayashi, Yoshihiro Murata, Osamu Seguchi, Masanobu Yanase, Yumiko Hori, Kyoichi Wada, Hatsue Ueda, Shigeki Miyata, Hiroaki Naito

Since the organ transplantation law was passed, we performed 50 heart transplantation at National Cerebral and Cardiovascular Center. Of those, 2 patients have been doing well over 13 years and 10 years survival rate was 93.4%. During those years, we performed 139 applications of left ventricular assist systems (LVAS). Initially, extracorporeal LVASs had been used. Now, 2 implantable LVAS were approved by medical insurance as bridge to transplant in 2011. Now, our 1st option as bridge to transplantation (BTT) is implantable LVAS.

KEY WORDS

heart transplantation/ventricular assist system/bridge to transplantation

*　　*　　*

次号予告〔66巻2号（2月号）〕

〈胸部外科の指針〉

■肺癌手術例における低用量未分画 heparin の術後肺塞栓症予防効果と安全性の長期成績

村岡昌司（諫早総合病院呼吸器外科）

▶**討論 1.** 谷田達男（岩手医科大学呼吸器外科）

▶**討論 2.** 土田正則（新潟大学第二外科）

〈今月の臨床〉

■再発性人工弁感染，大動脈弁輪膿瘍の播種性血管内凝固症候群に対する thrombomodulin-α の早期導入有効例

増田信也（東北大学心臓血管外科）

Tmem100, an ALK1 receptor signaling-dependent gene essential for arterial endothelium differentiation and vascular morphogenesis

Satoshi Somekawa[a,b], Keiichi Imagawa[a], Hisaki Hayashi[c], Masahide Sakabe[c], Tomoko Ioka[c], Genki E. Sato[c], Ken Inada[c], Takaaki Iwamoto[d], Toshio Mori[d], Shiro Uemura[a], Osamu Nakagawa[c,1], and Yoshihiko Saito[a,b]

[a]First Department of Internal Medicine, [b]Department of Regulatory Medicine for Blood Pressure, Nara Medical University, Kashihara, Nara, 634-8522, Japan; and [c]Laboratory for Cardiovascular System Research and [d]Radioisotope Research Center, Nara Medical University Advanced Medical Research Center, Kashihara, Nara, 634-8521, Japan

Edited by Eric N. Olson, University of Texas Southwestern Medical Center, Dallas, TX, and approved June 12, 2012 (received for review May 1, 2012)

Members of the transforming growth factor-β superfamily play essential roles in various aspects of embryonic development and physiological organ function. Among them, bone morphogenetic protein (BMP) 9 and BMP10 regulate embryonic vascular development by activating their endothelial receptor ALK1 (activin receptor-like kinase 1, also called Acvrl1). ALK1-mediated intracellular signaling is implicated in the etiologies of human diseases, but their downstream functional proteins are largely unknown. In this study, we identified *Tmem100*, a gene encoding a previously uncharacterized intracellular transmembrane protein, to be an embryonic endothelium-enriched gene activated by BMP9 and BMP10 through the ALK1 receptor. *Tmem100* null mice showed embryonic lethality due to impaired differentiation of arterial endothelium and defects of vascular morphogenesis, which phenocopied most of the vascular abnormalities observed with the *Acvrl1/Alk1* deficiency. The activity of Notch- and Akt-mediated signaling, which is essential for vascular development, was down-regulated in *Tmem100* null mice. *Cre*-mediated deletion of *Tmem100* in endothelial cells was sufficient to recapitulate the null phenotypes. These data indicated that TMEM100 may play indispensable roles downstream of BMP9/BMP10-ALK1 signaling during endothelial differentiation and vascular morphogenesis.

Formation of the cardiovascular network is essential for proper embryonic development, and neovascularization is associated with various adult diseases, such as ischemic heart diseases, retinopathy, and cancer, acting either protectively or deterioratively in those pathological states (1, 2). At early embryonic stages, vasculogenesis occurs as a de novo organization of endothelial cell plexus. A series of processes for vascular remodeling and maturation follows, including an initial phase of endothelial cell migration, proliferation, and tubular reorganization, collectively called angiogenesis, and a maturation phase when the structure of blood vessels is established by the stabilization of endothelial cells, acquirement of arterial or venous identity, and recruitment of mural cells to vascular walls (1, 2).

A variety of cellular signaling pathways controlling vascular development involve cytokines and growth factors, such as vascular endothelial growth factors (VEGFs), angiopoietins, transforming growth factor β (TGF-β), and bone morphogenetic proteins (BMPs) (3, 4). Among them, BMP9 and BMP10 act mainly through an endothelium-specific ALK1 (activin receptor-like kinase 1) receptor and promote arterial endothelial maturation and quiescence (5–7). Targeting disruption of the genes for the ALK1 receptor, a type III coreceptor endoglin, and downstream signaling components such as Tak1/Map3k7 caused embryonic lethality with remarkably similar defects of arterial endothelium differentiation and vascular morphogenesis (8–11). Despite clear demonstration of its critical roles in embryonic development, endothelial functional proteins downstream of the BMP9/BMP10-ALK1 signaling pathway remained unclear.

In a microarray screen to search for endothelial genes downstream of BMP9/BMP10-ALK1 signaling, we found that the expression of *Tmem100*, a gene encoding an intracellular transmembrane protein of unknown functions, was markedly augmented by BMP9 and BMP10. It was recently reported that *Tmem100* mRNA expression significantly decreased in the lung of *Acvrl1/Alk1* conditional knockout mice and that *Tmem100* drove endothelial-enriched expression of lacZ reporter in mouse embryos (12). In this paper, we demonstrated that *Tmem100* null mice and endothelial-specific *Tmem100* knockout mice showed fatal defects of arterial endothelium differentiation and vascular morphogenesis, which are virtually identical to the abnormalities due to the *Acvrl1/Alk1* deficiency. These results suggest that TMEM100 may play essential roles as a downstream target protein of BMP9/BMP10-ALK1 signaling in embryonic vascular development.

Results

***Tmem100*: An Arterial Endothelium-Enriched Gene Downstream of BMP9/BMP10-ALK1 Signaling.** In an attempt to identify endothelial genes downstream of BMP9/BMP10-ALK1 signaling, we first analyzed whether human umbilical artery endothelial cells (HUAEC) responded to the treatment with various TGF-β–related factors. Among several ligands tested, BMP9 potently stimulated the phosphorylation of Smad1/5/8 (Fig. S1 *A* and *B*). We then compared gene expression profiles of BMP9-treated HUAEC and control cells by an RNA microarray analysis (Fig. S1*C*). In addition to known BMP9-target genes such as *SMAD6*, *SMAD7*, *ID1*, and *ID2*, we found that *TMEM100* showed a marked activation of mRNA expression by the BMP9 treatment (Fig. 1*A*). Quantitative RT-PCR and Western blot analysis confirmed a dose-dependent induction of the *TMEM100* expression by BMP9, up to more than 100-fold (Fig. 1*A*). Similar levels of activation were observed with BMP10 (Fig. S1*D*), and those effects were significantly inhibited by knockdown of *ACVRL1/ALK1*, *BMPR2*, and *SMAD4* (Fig. 1*B* and Fig. S1*E*). These results indicated that BMP9/BMP10-induced *TMEM100* expression occurred through the ALK1/BMPR2 receptor complex and Smad-mediated transcriptional regulation.

TMEM100 is a gene encoding a protein with two putative transmembrane domains, but its physiological significance has not been described. The structure of TMEM100 protein is highly

Author contributions: S.S., O.N., and Y.S. designed research; S.S., K. Imagawa, H.H., M.S., T. Ioka, G.E.S., K. Inada, T. Iwamoto, and T.M. performed research; S.S., S.U., O.N., and Y.S. analyzed data; and S.S., O.N., and Y.S. wrote the paper.

The authors declare no conflict of interest.

This article is a PNAS Direct Submission.

[1]To whom correspondence should be addressed. E-mail: nakagawa-nmu@umin.org

This article contains supporting information online at www.pnas.org/lookup/suppl/doi:10.1073/pnas.1207210109/-/DCSupplemental.

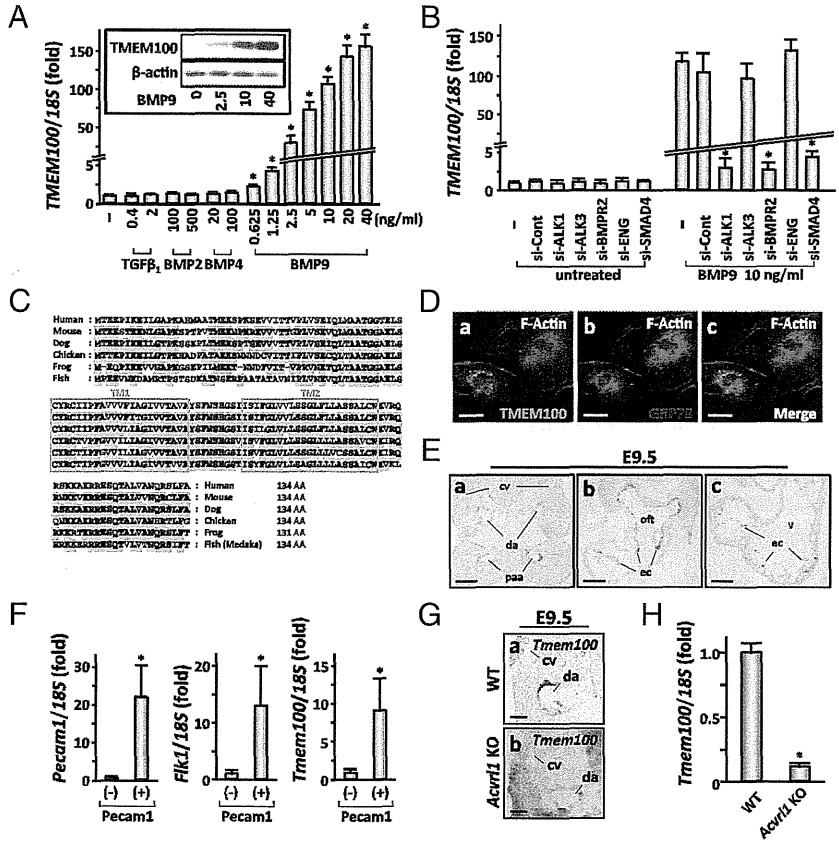

Fig. 1. *Tmem100*: an arterial endothelium-enriched gene downstream of BMP9/BMP10-ALK1 signaling. (*A*) BMP9 markedly increases *TMEM100* mRNA expression at 24 h in a dose-dependent manner. Quantitative RT-PCR analysis is shown. Fold increase relative to the untreated cells is shown with SD. (*Inset*) Western blot result shows a dose-dependent increase in TMEM100 protein expression. –, untreated. (*B*) BMP9-induced *TMEM100* mRNA expression is inhibited by pretreatment with ACVRL1/ALK1 siRNA (si-ALK1), BMPR2 siRNA (si-BMPR2), or SMAD4 siRNA (si-SMAD4), but not with BMPR1A/ALK3 siRNA (si-ALK3), Endoglin siRNA (si-ENG), or control siRNA (si-Cont). Quantitative RT-PCR is shown. –, untreated. (*C*) Amino acid sequences of TMEM100 from various species. Boxes represent two putative transmembrane (TM) domains. Residues conserved with the human sequence are shaded in gray. (*D*) TMEM100 protein predominantly resides in the perinuclear region overlapping endoplasmic reticulum marked by anti-GRP78/HSPA5 antibody. Immunocytochemistry of HUAEC transfected with a TMEM100-FLAG expression plasmid is shown. (*E*) *Tmem100* mRNA is expressed specifically in arterial endothelial cells of pharyngeal arch artery (paa) and dorsal aorta (da) as well as in endocardium (ec), but not in cardinal vein (cv), at E9.5. In situ hybridization is shown. oft, outflow tract; v, ventricle. (*F*) *Tmem100* expression is enriched in endothelial cells also at earlier developmental stages. Shown is FACS sorting of Pecam1-positive cells from E8.5 embryos followed by quantitative RT-PCR. *Pecam1* and *Kdr/Flk1* expression was examined to confirm proper selection of the endothelial population. (*G*) *Tmem100* expression in dorsal aorta is reduced in *Acvrl1/Alk1* null embryos at E9.5. In situ hybridization is shown. (*H*) *Tmem100* expression significantly decreases in the yolk sac of *Acvrl1/Alk1* null mice at E9.5. Quantitative RT-PCR is shown. In *A*, *B*, *F*, and *H*, asterisks indicate data with statistical significance (*$P < 0.05$). (Scale bars: *D*, 10 μm; *E*, 50 μm; and *G*, 20 μm.)

conserved from fish to humans, especially in its putative transmembrane domains (Fig. 1*C*); however, no structurally related family of proteins was found in any species, indicating that TMEM100 represents a previously uncharacterized entity of functional proteins. Levels of endogenous TMEM100 expression in HUAEC were below detection limits in immunocytochemical analyses, whereas TMEM100 protein expressed using a mammalian expression plasmid resided in the perinuclear region marked by endoplasmic reticulum (ER) proteins such as GRP78/HSPA5 (Fig. 1*D* and Fig. S2*A*). Endogenous TMEM100 protein in BMP9-treated HUAEC was recovered to the subcellular membrane fraction and was enriched in the ER microsome (Fig. S2 *B* and *C*). In adult mice, *Tmem100* was most abundantly expressed in the lung with a lower level of expression in the brain, heart, and muscle (Fig. S2*D*). In mouse embryos, *Tmem100* mRNA was detected from embryonic day (E) 8.5 (Fig. S2*E*) and was enriched in arterial endothelium and endocardium (Fig. 1*E* and see Fig. S4*A*). Quantitative RT-PCR confirmed the enrichment of *Tmem100* mRNA in the platelet/endothelial cell adhesion molecule 1 (Pecam1)-positive endothelial cell population sorted from E8.5 embryos (Fig. 1*F*). Consistent with ALK1-mediated *Tmem100* expression in HUAEC (Fig. 1 *A* and *B*) and the previous report (12), *Tmem100* mRNA expression in arterial endothelium was significantly reduced in *Acvrl1/Alk1* null embryos (Fig. 1 *G* and *H*).

These results prompted us to examine functional significance of TMEM100 in vascular differentiation and morphogenesis during development.

Embryonic Lethality by Targeted Disruption of *Tmem100*. We generated *Tmem100*-deficient mice in which exon 3 encoding the entire coding region was replaced with a lacZ-neo cassette (Fig. S3 *A*–*C*). Mice heterozygous for the *Tmem100* mutation survived to adulthood and were fertile. LacZ reporter driven by the *Tmem100* locus (*Tmem100-lacZ*) was predominantly expressed in developing arteries, including dorsal aorta and pharyngeal arch; intersomitic, umbilical, and vitelline arteries; and endocardium (Fig. 2 *A* and *B* and Fig. S4 *B*–*D*). Vascular expression of *Tmem100-lacZ* overlapped with that of lacZ reporter knocked into the *Acvrl1/Alk1* locus (Fig. 2 *A* and *B*) and was observed in

DEVELOPMENTAL BIOLOGY

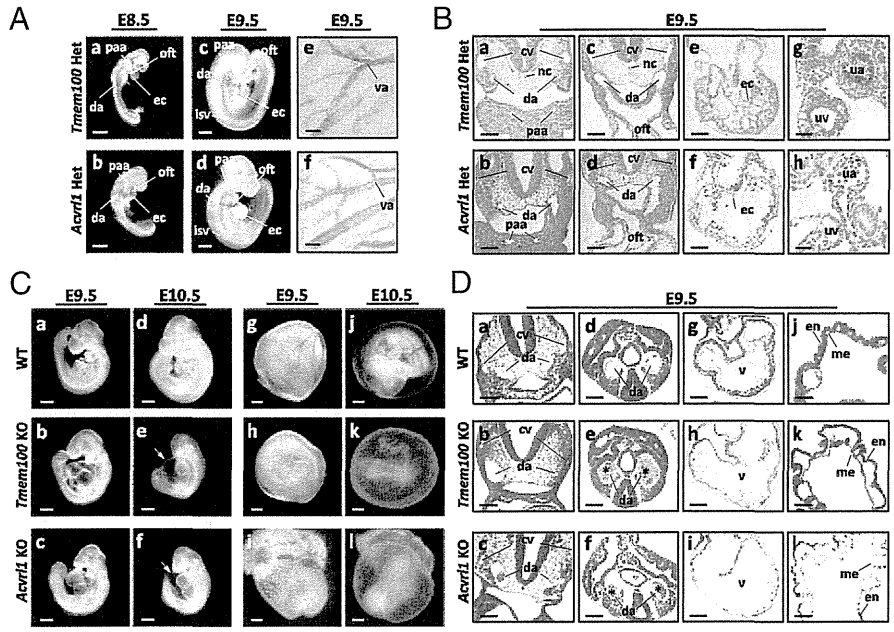

Fig. 2. *Tmem100* and *Acvrl1/Alk1*: arterial expression of knock-in lacZ reporter and angiogenesis defects in null embryos. (*A* and *B*) Knock-in lacZ reporter activity is detected in major arteries and endocardium in both *Tmem100* and *Acvrl1/Alk1* heterozygous mice. Sections counterstained with nuclear fast red are shown in *B*. (C) *Tmem100* null embryos die in utero, showing cardiac dysmorphogenesis and enlargement at E9.5, massive pericardial effusion (arrow) and severe growth retardation at E10.5, and absence of large vitelline vessels in the yolk sac at E10.5. These phenotypes are also observed in *Acvrl1/Alk1* null embryos. (*D*) *Tmem100* null and *Acvrl1/Alk1* null embryos have remarkably similar defects of cardiovascular morphogenesis. Paired dorsal aortas show marked dilatation and narrowing, and clumps of blood cells are frequently seen in the caudal region (asterisk). Mural layers surrounding the aorta and myocardial wall are thinner and ventricular trabeculation is not formed well. The yolk sac shows detachment of endodermal (en) and mesodermal (me) layers and abnormal vessel dilatation. H&E staining at E9.5 is shown. cv, cardinal vein; da, dorsal aorta; isv, intersomitic vessel; nc, notochord; oft, outflow tract; paa, pharyngeal arch artery; ua, umbilical artery; uv, umbilical vein; v, ventricle; va, vitelline artery. (Scale bars: *A*, *a–d*, and *C*, 200 μm; *A*, e and *f*, *B*, a–f, and *D*, *a–i*, 50 μm; and *B*, *g* and *h*, and *D*, *j–l*, 20 μm.)

the endothelial layer of dorsal aorta but not in smooth muscle cells (Fig. S4 *C* and *D*). At later embryonic stages, *Tmem100-lacZ* expression was also detected in the limb buds, somites, and other tissues (Fig. S4*B*). In the adult lung, *lacZ* reporter was expressed in vascular endothelial cells as well as in alveolar cells (Fig. S4*E*).

Breeding of heterozygous mice revealed a significant deviation from expected inheritance, and no surviving embryos were recovered at and after E11.0 (Fig. S3*D*). *Tmem100* null embryos at E10.5 were strongly affected, showing abnormal cardiac morphology, massive pericardial effusion, and growth retardation (Fig. 2*C*), suggesting that cardiovascular failure caused embryonic lethality of *Tmem100* null mice.

Vascular Defects in *Tmem100* Null Mice. *Tmem100* null embryos showed no detectable phenotypes until E8.5, and the formation of primitive vasculature appeared normal (Fig. S5*A*). Earliest signs of deficiency were observed in the vasculature at E9.0–9.5. The yolk sac of *Tmem100* null embryos showed reduction of vitelline circulation (Fig. 2*C*). Consistently, *Tmem100* null embryos displayed a variety of severe abnormalities in vascular morphology, as shown in Fig. 2*D*. One of the paired dorsal aortae frequently showed a marked dilatation with a narrowing or closure on the opposite side, and clumps of blood cells were often observed in the caudal region, which is likely to be due to vascular obstruction. Cardiac myocardium was thinner, and the yolk sacs showed detachment of endodermal and mesodermal layers and abnormal vessel dilatation (Fig. 2*D*).

Whole-mount Pecam1 staining revealed abnormally coarse vascular patterns, indicative of impaired vascular remodeling (Fig. 3*A*), and India ink injection identified arteriovenous malformation from dorsal aorta toward sinus venosus in *Tmem100* null embryos (Fig. 3*B* and Fig. S5*B*). These phenotypes of *Tmem100* null embryos were mostly identical to those observed in *Acvrl1/Alk1* null embryos (Fig. 2 *C* and *D* and Fig. S6*A*) and reported in previous studies (8, 9).

Defects of Arterial Differentiation in *Tmem100* Null Embryos. ALK1-mediated signaling is implicated in establishing arterial identity of vascular endothelial cells (8, 9). Indeed, the expression of arterial marker genes *Efnb2* and *Gja5/Cx40* was significantly decreased in dorsal aorta of *Tmem100* null embryos as early as E8.5 (Fig. 3 *C* and *D*). In contrast, expression of *Cdh5* (encoding VE-cadherin), *Kdr/Flk1*, and *Pecam1* was maintained (Fig. 3 *C–E*), suggesting that arterial specification is compromised by *Tmem100* deficiency. Upon normal arterial maturation, mural smooth muscle precursors marked by Sm22 are recruited (1, 2); however, the *Sm22/Tagln* expression around the dorsal aorta was significantly reduced in *Tmem100* null embryos (Fig. 3*F*). These defects of arterial differentiation and maturation were also observed in *Acvrl1/Alk1* null mice (Fig. S6 *B–E*).

Down-Regulation of Endothelial Signaling Pathways in *Tmem100* Null Embryos. To begin to understand mechanisms of vascular abnormalities caused by the *Tmem100* deficiency, we performed a microarray analysis using the yolk sac, which is a vascular-rich tissue with obvious null phenotypes (Fig. S7*A*). We observed a significant decrease in the expression of arterial markers, such as *Efnb2*, *Gja4/Cx37*, and *Gja5/Cx40*, and an increase in vein-specific *Ephb4* expression in the *Tmem100* null yolk sac (Fig. 4*A* and Fig. S7*B*), which is consistent with our notion that *Tmem100* is essential for arterial endothelium differentiation.

We also found that the expression of Notch downstream genes *Hrt1/Hey1*, *Hrt2/Hey2*, *Hrt3/Heyl*, and *Hes5* (13, 14) was signifi-

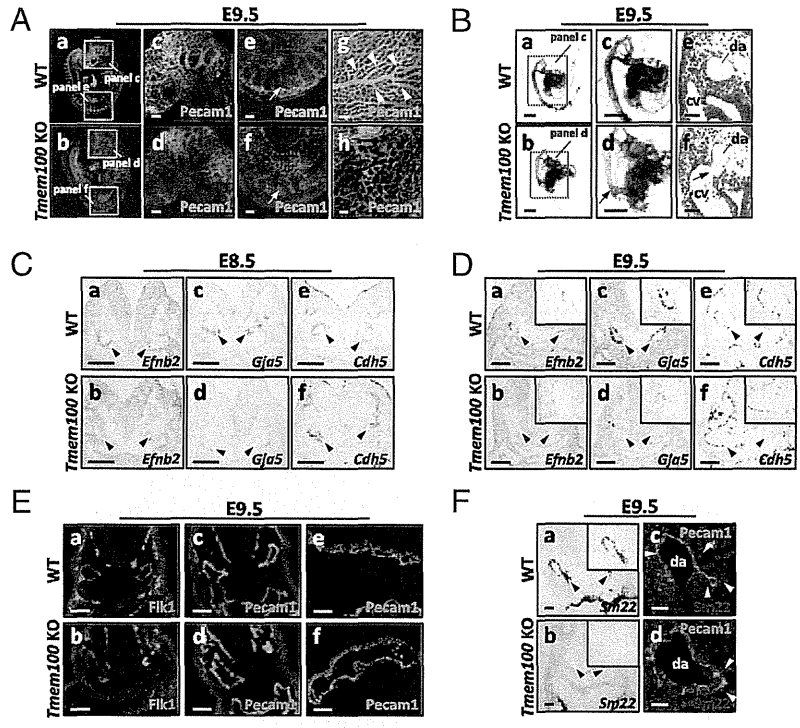

Fig. 3. Impairment of vascular remodeling and arterial endothelium differentiation in *Tmem100* null embryos. (*A*) Impaired vascular remodeling is visualized by whole-mount Pecam1 immunostaining in the *Tmem100* null embryos (*b*, *d*, and *f*) and yolk sac (*h*). Arrows indicate intersomitic vessels. Arrowheads indicate highly organized vascular branches in the wild-type yolk sac. *a–f* are shown with nuclear DAPI stain. (*B*) Abnormal vascular connections (arrow) between dorsal aorta and cardinal veins are observed in null embryos. Shown is microangiography by India ink injection and H&E staining. (*C* and *D*) Expression of arterial endothelium marker genes *Efnb2* and *Gja5/Cx40* diminishes in dorsal aorta (arrowheads) of *Tmem100* null embryos at E8.5 (*C*) and E9.5 (*D*), whereas maintenance of *Cdh5* expression indicates existence of endothelial layers. In situ hybridization is shown. (*E*) Flk1 and Pecam1 expression is preserved in dorsal aorta of *Tmem100* null embryo (*b* and *d*) and yolk sac vasculature (*f*). Immunohistochemistry with nuclear DAPI stain is shown. (*F*) Expression of *Sm22/Tagln* mRNA and SM22 protein in the mural layers of dorsal aorta is significantly reduced in *Tmem100* null embryos (arrowheads). In situ hybridization (*a* and *b*) and immunohistochemistry with nuclear DAPI stain (*c* and *d*) are shown. *Insets* in *D* and *F* show magnified views of dorsal aorta. (Scale bars: *A*, *C*, *D*, and *E*, *a–d*, 50 μm; *B*, *a–d*, 200 μm; and *B*, e and *f*, *E*, e and *f*, and *F*, 20 μm.)

cantly decreased in *Tmem100* null yolk sac (Fig. 4*A* and Fig. S7*C*). Because Notch signaling was known to be essential for arterial differentiation (1, 2, 15), we further examined whether the activity of Notch signaling is down-regulated in *Tmem100* null embryos. Upon activation by the ligands such as Delta and Jagged, the intracellular domain of Notch receptors, NICD, is enzymatically cleaved and translocated to the nucleus, where it forms a transcriptional activator complex with RBP-J and other cofactors (14). Western blot analysis demonstrated a significant decrement of NICD expression in *Tmem100* null embryos and yolk sac (Fig. 4*B*). Immunohistochemical staining using an anti–NICD-specific antibody indicated that down-regulation of NICD expression was specific to the arterial endothelium and endocardium and was not observed in other Notch-regulated tissues such as somite and neural tube (Fig. 4*C*). The total amount of Notch receptors, which was examined using an antibody recognizing both full-length Notch receptors and NICD, appeared unchanged (Fig. 4*D*). Furthermore, the expression of Notch-target transcription factor Hrt2/Hey2 was significantly decreased in the vasculature of *Tmem100* null embryos, whereas its expression in the cardiac muscle was unaltered (Fig. 4*E*).

In addition, we observed a decrease in Akt phosphorylation in *Tmem100* null embryos and yolk sac (Fig. 4*B*). Consistently, the expression of *Klf2* and *eNOS/Nos3* (Fig. 4*A*) and the cleavage of Presenilin-1 (Ps1) (Fig. 4*F*), which can be activated by Akt signaling (16–18), were suppressed in null embryos and yolk sac, suggesting down-regulation of Akt-mediated signaling important for endothelial survival, migration, and homeostasis. Importantly, dysregulation of Notch and Akt signaling was also observed in *Acvrl1/Alk1* null mice (Fig. S6 *F–K*).

In contrast, other signaling pathways implicated in embryonic vascular development did not appear compromised (1, 2, 19–22). The levels of ERK and Smad1/5/8 phosphorylation did not alter in *Tmem100* null embryos and yolk sac (Fig. S7 *D–F*). Components of Angiopoietin, Hedgehog, Semaphorin, and fibroblast growth factor signaling pathways and their downstream target genes did not show aberrant expression in *Tmem100* null yolk sac (Fig. S7*C*). These data suggested that the *Tmem100* deficiency caused impairment of arterial differentiation and morphogenesis through, at least in part, down-regulation of Notch- and Akt-mediated signaling.

Embryonic Vascular Defects by Cre-Mediated Deletion of *Tmem100* in Endothelial Cells. We further examined phenotypes of the mice with *Tek-Cre*–mediated endothelial cell-specific deletion of the *Tmem100* gene (Fig. S8 *A–D*). Endothelial-specific deletion of *Tmem100* caused vascular defects remarkably similar to those observed in global *Tmem100* null mice and embryonic lethality around E11.0 (Fig. S8 *E* and *F*). Expression of arterial endothelium-specific genes and a vascular smooth muscle marker SM22 apparently decreased, and Notch- and Akt-mediated signaling was down-regulated also by the endothelial-specific *Tmem100* deletion (Fig. S9 *A–D*). These results indicated that the endothelial expression of *Tmem100* is essential for arterial differentiation and embryonic development.

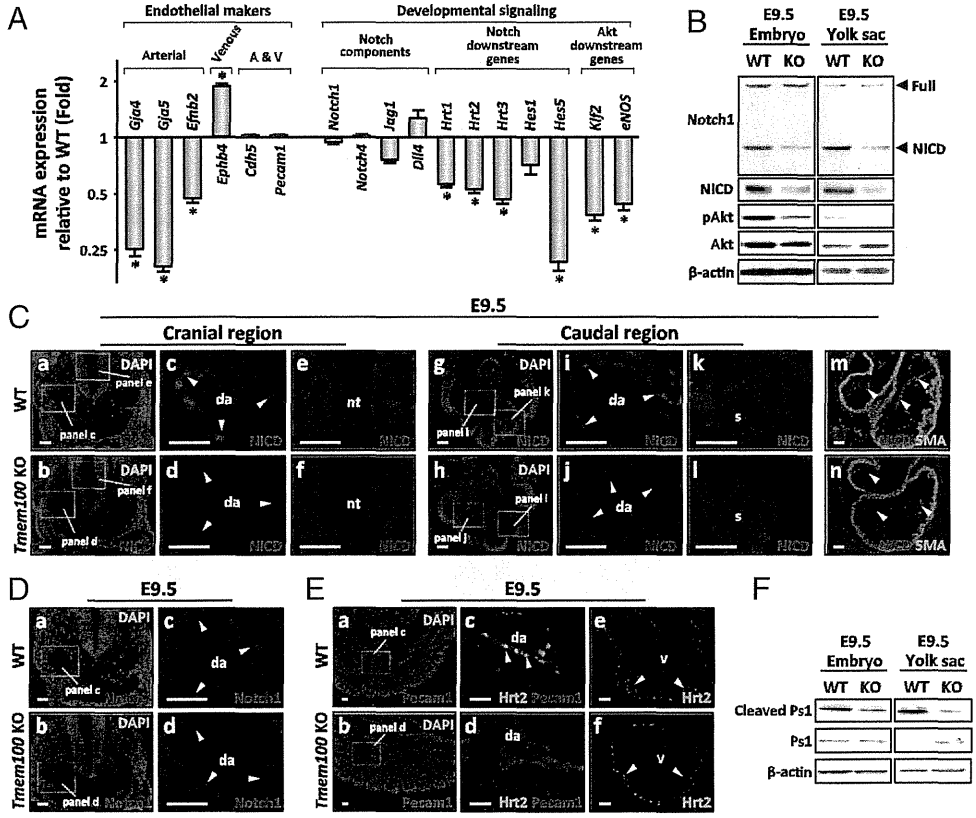

Fig. 4. Notch- and Akt-mediated signaling pathways are down-regulated in *Tmem100* null embryos and yolk sac. (*A*) Expression of arterial endothelium markers, Notch downstream genes, and Akt downstream genes markedly decreases in *Tmem100* null yolk sac at E9.5. Expression of a venous endothelium marker, *Ephb4*, is significantly up-regulated. Quantitative RT-PCR is shown. (*B*) The amount of the intracellular domain of Notch receptor (NICD) and phosphorylated Akt significantly decreases in *Tmem100* null embryos and yolk sac at E9.5, whereas that of full-length Notch1 receptor and total Akt remains unchanged. Western blot analysis is shown. (*C*) NICD expression markedly decreases in dorsal aorta (da) and endocardium (arrowheads in *d*, *j*, and *n*), but not in the neural tube (nt) and somites (s) (*f* and *l*), of E9.5 null embryos. Immunohistochemistry using a NICD-specific antibody is shown. *a*, *b*, *g*, *h*, *m*, and *n* are shown with nuclear DAPI stain. (*D*) Total amount of Notch receptors does not decrease in vascular endothelium of null embryos. Immunohistochemistry using an antibody recognizing full-length Notch receptors and NICD is shown. *a* and *b* are shown with nuclear DAPI stain. (*E*) Expression of Hrt2, a Notch downstream transcription factor, significantly decreases in the vasculature of *Tmem100* null embryos (*d*), whereas its expression in cardiac muscle was unchanged (*f*). Immunohistochemistry is shown. *a* and *b* are shown with nuclear DAPI stain. (*F*) Cleaved Presenilin-1 (Ps1) decreases in null embryos and yolk sac at E9.5. Western blot analysis is shown. (Scale bars in *C–E*, 20 μm.)

Discussion

In searching for genes involved in the regulation of endothelial differentiation and vascular development, we identified *Tmem100* to be a gene activated downstream of BMP9/BMP10-ALK1 signaling. *Tmem100* and *Acvrl1/Alk1* were expressed in arterial endothelial cells during vascular development in mouse embryos, and their targeting disruption caused embryonic lethality with remarkably similar abnormalities of arterial endothelium differentiation and vascular morphogenesis. *Tmem100* expression significantly decreased in *Acvrl1/Alk1* null embryos, which is consistent with down-regulation of *Tmem100* expression in the adult lung of *Acvrl1/Alk1* conditional knockout mice (12). It has not been studied whether BMP9 and BMP10 are major regulators of *Tmem100* expression in vivo. *Bmp10* null mice show impaired cardiac growth but not defects of angiogenesis (23), whereas the phenotypes of *Gdf2* (encoding BMP9) knockout mice have not been reported. Examining whether the mice null for both *Gdf2* and *Bmp10* show embryonic vascular defects will provide further insights into in vivo regulatory mechanisms of *Tmem100* expression.

Notch-mediated signaling was suppressed in arterial endothelium of *Tmem100* null embryos as well as in endothelial-specific *Tmem100* knockout embryos. We also found that Notch signaling was down-regulated in *Acvrl1/Alk1* null embryos. Notch receptors and ligands are enriched in arterial but not venous endothelium of mouse embryos, and target disruption of Notch signaling components such as *Notch1*, *Notch4*, *Dll4*, *Rbpj*, *Hrt1/Hey1*, and *Hrt2/Hey2* revealed that Notch activity is crucial for promoting arterial cell fate (1, 2, 15). Impairment of endothelial Notch signaling affects vascular smooth muscle cell recruitment or differentiation during arterial maturation (24–26), which was observed in *Tmem100* and *Acvrl1/Alk1* knockout mice in the present study. In addition to Notch signaling, the activities of Akt kinase and Ps1 protease appeared repressed in *Tmem100* and *Acvrl1/Alk1* knockout embryos. It was reported that Akt enhances Ps1-mediated Notch cleavage (16, 27) and that Ps1 provokes Akt activation in turn (28). The signaling relay or mutual interaction involving Akt, Ps1, and Notch might play a role in the pathogenesis of vascular defects by the *Tmem100* and *Acvrl1/Alk1* deficiency.

A number of biological stimuli including fluid shear stress could influence Akt- and Notch-mediated signaling as a result of insufficient circulation (1, 2, 15). Markers of arterial endothelium differentiation, however, became down-regulated before apparent structural abnormalities in *Tmem100* null embryos, suggesting a possibility that TMEM100 is directly involved in acquiring arterial cell fate. Previous studies reported *Tmem100*

expression in embryonic vasculature and the adult lung, prostate, and kidney in humans and mice (12, 29, 30), but cellular functions of TMEM100 have not been investigated. We found that TMEM100 protein was mainly localized in ER, but not in plasma membrane, of cultured endothelial cells. It is tempting to speculate that TMEM100 works for posttranslational protein modification or intracellular sorting in the membrane of ER and surrounding structures. Elucidating molecular functions of TMEM100 is essential to clarify how TMEM100 conveys the BMP9/BMP10-ALK1 signals toward the downstream signaling cascade for proper endothelial differentiation.

Mutations in *ACVRL1/ALK1*, *BMPR2*, *ENG*, or *SMAD4* cause hereditary hemorrhagic telangiectasia as well as pulmonary arterial hypertension in humans (31, 32). *TMEM100* might be involved in the mechanisms of these diseases as an additional causative gene or a modifier. At late embryonic and adult stages, *Tmem100* expression appears to be not restricted to vascular endothelial cells. Studying the significance of TMEM100 may lead to a better understanding of human diseases in the cardiovascular system and other organs.

Materials and Methods

Cell Culture and Microarray Analysis. HUAEC (Takara Bio) were precultured in Endothelial Basal Medium 2 medium with 0.2% FBS for 3 h and treated with TGF-β superfamily ligands (R&D Systems) for 24 h. siRNA was electroporated to HUAEC 36 h before the BMP9 or BMP10 treatment. Other cell culture experiments were performed using standard procedures.

Two-color microarray analyses using the human and mouse whole-genome 4x44K v2 oligo microarray systems (Agilent Technologies) were performed to examine mRNA expression profiles of BMP9-treated HUAEC and the yolk sac of *Tmem100* null mice, respectively.

Generation of *Tmem100* Null Mice. The *Tmem100*-lacZ targeting vector was constructed using a BAC clone containing the *Tmem100* locus genomic DNA (BACPAC Resources) and was electroporated into C57BL/6 embryonic stem cells for homologous recombination (Fig. S3*A*). A correctly targeted clone, as identified by Southern blot analysis, was injected into BALB/c blastocysts. Chimeras were bred to obtain heterozygous mice that carry the targeted *Tmem100* locus in their germ line. The floxed PGK-neo cassette was removed by breeding with a *CAG-Cre* transgenic line. All breeding was done with mice under the C57BL/6 genetic background. Procedures to generate mice for conditional *Tmem100* deletion are described in *SI Materials and Methods*. All animal experiments were approved by the institutional committee.

Biochemical, Histological, and Anatomical Analyses. Quantitative RT-PCR, Northern blot analysis, Western blot analysis, in situ hybridization, immunohistochemistry, and lacZ staining were performed using standard procedures. A rabbit polyclonal antibody generated against a carboxyl-terminal 27-aa fragment of mouse TMEM100 protein was used for Western blot analysis of HUAEC. Details of PCR primers, Northern probe, and primary antibodies are described in *SI Materials and Methods*. Microangiography was performed by India ink injection to the outflow tract of mouse embryos.

ACKNOWLEDGMENTS. The authors thank Drs. E. Olson, J. Hill, and P. ten Dijke for profitable advice and support. The authors also thank Drs. A. Wanaka, K. Tatsumi, H. Yamagishi, K. Uchida, H. Bannai, H. Kurihara, R. Asai, S. Itoh, F. Itoh, T. Morioka, and M. Itoh for experimental information and Ms. M. Ikugawa, T. Fujita, Y. Yoshioka, and M. Sakaida for technical assistance. This study was supported in part by grants from the Ministry of Education, Culture, Sports, Science, and Technology (to O.N., S.S., H.H., M.S., and Y.S.); grants from the Astellas Foundation for Research on Metabolic Disorders, the Mitsubishi Pharma Research Foundation, the Miyata Cardiac Research Promotion Foundation, Novartis Foundation (Japan) for the Promotion of Science, Suzuken Memorial Foundation, the Takeda Science Foundation, The Mother and Child Health Foundation, The Naito Foundation, The Smoking Research Foundation, and the Uehara Memorial Foundation (to O.N.); grants from the Banyu Life Science International Foundation and Takeda Science Foundation (to S.S.); grants from the Takeda Science Foundation, The Ichiro Kanahara Foundation, and The Nakatomi Foundation (to H.H.); a grant from Japan Heart Foundation (to M.S.); and a research grant for Cardiovascular Diseases (20A-3) from the Ministry of Health, Labor and Welfare (to Y.S.).

1. Potente M, Gerhardt H, Carmeliet P (2011) Basic and therapeutic aspects of angiogenesis. *Cell* 146:873–887.
2. Eilken HM, Adams RH (2010) Dynamics of endothelial cell behavior in sprouting angiogenesis. *Curr Opin Cell Biol* 22:617–625.
3. David L, Feige JJ, Bailly S (2009) Emerging role of bone morphogenetic proteins in angiogenesis. *Cytokine Growth Factor Rev* 20:203–212.
4. Pardali E, Goumans MJ, ten Dijke P (2010) Signaling by members of the TGF-beta family in vascular morphogenesis and disease. *Trends Cell Biol* 20:556–567.
5. David L, Mallet C, Mazerbourg S, Feige JJ, Bailly S (2007) Identification of BMP9 and BMP10 as functional activators of the orphan activin receptor-like kinase 1 (ALK1) in endothelial cells. *Blood* 109:1953–1961.
6. Scharpfenecker M, et al. (2007) BMP-9 signals via ALK1 and inhibits bFGF-induced endothelial cell proliferation and VEGF-stimulated angiogenesis. *J Cell Sci* 120:964–972.
7. Suzuki Y, et al. (2010) BMP-9 induces proliferation of multiple types of endothelial cells in vitro and in vivo. *J Cell Sci* 123:1684–1692.
8. Urness LD, Sorensen LK, Li DY (2000) Arteriovenous malformations in mice lacking activin receptor-like kinase-1. *Nat Genet* 26:328–331.
9. Oh SP, et al. (2000) Activin receptor-like kinase 1 modulates transforming growth factor-beta 1 signaling in the regulation of angiogenesis. *Proc Natl Acad Sci USA* 97:2626–2631.
10. Li DY, et al. (1999) Defective angiogenesis in mice lacking endoglin. *Science* 284:1534–1537.
11. Jadrich JL, O'Connor MB, Coucouvanis E (2006) The TGF beta activated kinase TAK1 regulates vascular development in vivo. *Development* 133:1529–1541.
12. Moon EH, et al. (2010) Generation of mice with a conditional and reporter allele for Tmem100. *Genesis* 48:673–678.
13. Nakagawa O, et al. (2000) Members of the HRT family of basic helix-loop-helix proteins act as transcriptional repressors downstream of Notch signaling. *Proc Natl Acad Sci USA* 97:13655–13660.
14. Kopan R, Ilagan MX (2009) The canonical Notch signaling pathway: Unfolding the activation mechanism. *Cell* 137:216–233.
15. Swift MR, Weinstein BM (2009) Arterial-venous specification during development. *Circ Res* 104:576–588.
16. Takeshita K, et al. (2007) Critical role of endothelial Notch1 signaling in postnatal angiogenesis. *Circ Res* 100:70–78.
17. Sako K, et al. (2009) Angiopoietin-1 induces Kruppel-like factor 2 expression through a phosphoinositide 3-kinase/AKT-dependent activation of myocyte enhancer factor 2. *J Biol Chem* 284:5592–5601.
18. SenBanerjee S, et al. (2004) KLF2 is a novel transcriptional regulator of endothelial proinflammatory activation. *J Exp Med* 199:1305–1315.
19. Srinivasan R, et al. (2009) Erk1 and Erk2 regulate endothelial cell proliferation and migration during mouse embryonic angiogenesis. *PLoS ONE* 4:e8283.
20. Lechleider RJ, et al. (2001) Targeted mutagenesis of Smad1 reveals an essential role in chorioallantoic fusion. *Dev Biol* 240:157–167.
21. Yang X, et al. (1999) Angiogenesis defects and mesenchymal apoptosis in mice lacking SMAD5. *Development* 126:1571–1580.
22. Chang H, et al. (1999) Smad5 knockout mice die at mid-gestation due to multiple embryonic and extraembryonic defects. *Development* 126:1631–1642.
23. Chen H, et al. (2004) BMP10 is essential for maintaining cardiac growth during murine cardiogenesis. *Development* 131:2219–2231.
24. Morrow D, et al. (2008) Notch and vascular smooth muscle cell phenotype. *Circ Res* 103:1370–1382.
25. Fischer A, Schumacher N, Maier M, Sendtner M, Gessler M (2004) The Notch target genes Hey1 and Hey2 are required for embryonic vascular development. *Genes Dev* 18:901–911.
26. High FA, et al. (2008) Endothelial expression of the Notch ligand Jagged1 is required for vascular smooth muscle development. *Proc Natl Acad Sci USA* 105:1955–1959.
27. Yamamizu K, et al. (2010) Convergence of Notch and beta-catenin signaling induces arterial fate in vascular progenitors. *J Cell Biol* 189:325–338.
28. Baki L, et al. (2004) PS1 activates PI3K thus inhibiting GSK-3 activity and tau overphosphorylation: Effects of FAD mutations. *EMBO J* 23:2586–2596.
29. van der Heul-Nieuwenhuijsen L, Hendriksen PJ, van der Kwast TH, Jenster G (2006) Gene expression profiling of the human prostate zones. *BJU Int* 98:886–897.
30. Georgas K, et al. (2009) Analysis of early nephron patterning reveals a role for distal RV proliferation in fusion to the ureteric tip via a cap mesenchyme-derived connecting segment. *Dev Biol* 332:273–286.
31. Govani FS, Shovlin CL (2009) Hereditary haemorrhagic telangiectasia: A clinical and scientific review. *Eur J Hum Genet* 17:860–871.
32. Lowery JW, de Caestecker MP (2010) BMP signaling in vascular development and disease. *Cytokine Growth Factor Rev* 21:287–298.

EUROPEAN SOCIETY OF CARDIOLOGY®

Cardiovascular Research (2012) **96**, 433–443
doi:10.1093/cvr/cvs271

Enhanced binding of calmodulin to the ryanodine receptor corrects contractile dysfunction in failing hearts

Akihiro Hino[1], Masafumi Yano[1]*, Takayoshi Kato[1], Masakazu Fukuda[1], Takeshi Suetomi[1], Makoto Ono[1], Wakako Murakami[1], Takehisa Susa[1], Shinichi Okuda[1], Masahiro Doi[1], Shigeki Kobayashi[1], Takeshi Yamamoto[1], Noritaka Koseki[2], Hiroyuki Kyushiki[2], Noriaki Ikemoto[3,4], and Masunori Matsuzaki[1]

[1]Division of Cardiology, Department of Medicine and Clinical Science, Yamaguchi University Graduate School of Medicine, 1-1-1 Minamikogushi, Ube, Yamaguchi 755-8505, Japan; [2]First Institute of New Drug Discovery, Otsuka Pharmaceutical Co., Ltd, 463-10 Kagasuno Kawauchi-cho, Tokushima 771-0192, Japan; [3]Boston Biomedical Research Institute, Watertown, MA 02472, USA; and [4]Department of Neurology, Harvard Medical School, Boston, MA 02115, USA

Received 25 January 2012; revised 7 August 2012; accepted 8 August 2012; online publish-ahead-of-print 14 August 2012

Time for primary review: 43 days

Aims The channel function of the cardiac ryanodine receptor (RyR2) is modulated by calmodulin (CaM). However, the involvement of CaM in aberrant Ca^{2+} release in diseased hearts remains unclear. Here, we investigated the pathogenic role of defective CaM binding to the RyR2 in the channel dysfunction associated with heart failure.

Methods and results The involvement of CaM in aberrant Ca^{2+} release was assessed in normal and pacing-induced failing canine hearts. The apparent affinity of CaM for RyR2 was considerably lower in failing sarcoplasmic reticulum (SR) compared with normal SR. Thus, the amount of CaM bound to RyR2 was markedly decreased in failing myocytes. Expression of the CaM isoform Gly-Ser-His-CaM (GSH-CaM), which has much higher binding affinity than wild-type CaM for RyR1, restored normal CaM binding to RyR2 in both SR and myocytes of failing hearts. The Ca^{2+} spark frequency (SpF) was markedly higher and the SR Ca^{2+} content was lower in failing myocytes compared with normal myocytes. The incorporation of GSH-CaM into the failing myocytes corrected the aberrant SpF and SR Ca^{2+} content to normal levels.

Conclusion Reduced CaM binding to RyR2 seems to play a critical role in the pathogenesis of aberrant Ca^{2+} release in failing hearts. Correction of the reduced CaM binding to RyR2 stabilizes the RyR2 channel function and thereby restores normal Ca^{2+} handling and contractile function to failing hearts.

Keywords Calmodulin • Ryanodine receptor • Sarcoplasmic reticulum • Calcium • Heart failure

1. Introduction

The cardiac Ca^{2+} release channel of the sarcoplasmic reticulum (SR), referred to as the ryanodine receptor (RyR2), is a huge scaffolding protein that is known to release a large amount of Ca^{2+} synchronously, producing the transient Ca^{2+} elevations required for muscle contraction on a beat-to-beat basis.[1] In heart failure (HF), protein kinase A-dependent hyperphosphorylation and subsequent dissociation of RyR2-bound FKBP12.6,[2,3] as well as Ca^{2+}/calmodulin (CaM)-dependent protein kinase-II (CaMKII) activation, result in the leakage of Ca^{2+} through RyR2.[4,5] We have reported that in pacing-induced HF, the interaction between the N-terminal domain (aa 1–600) and the central domain (aa 2000–2500) of RyR2, which acts as an implicit on/off switch (designated as the domain switch) for channel opening and closing, is aberrantly weak, resulting in Ca^{2+} leakage.[6] We further demonstrated that oxidative stress is responsible for the defective inter-domain interaction and resultant Ca^{2+} leakage in failing hearts[7] and that either K201 or dantrolene, which bind the 2114–2149 and

* Corresponding author. Tel: +81 836 22 2248; fax: +81 836 22 2246, Email: yanoma@yamaguchi-u.ac.jp

601–620 regions of RyR2, respectively, can correct the configuration of the domain switch from the aberrant unzipped state to a normal zipped state, thus restoring normal inter-domain interaction and correcting diastolic Ca^{2+} leakage.[8,9]

CaM is one of the accessory proteins of RyR2. One molecule of CaM binds to one subunit of RyR2 in the normal state.[10] CaM binds to the 3583–3603 region of RyR2.[11] Meissner and colleagues[12] showed that RyR2-bound CaM was critical for normal muscle function and that CaM dissociation was involved in the pathogenesis of cardiac disorders. They generated a mouse with 3 amino acid substitutions in the CaM-binding domain (CaMBD) of RyR2 that abrogated the CaM binding to RyR2 and found that the mutant mouse developed hypertrophic cardiomyopathy with severely impaired contractile function and early death.[12]

In agreement with this report, we previously showed that RyR2-bound CaM, which acts essentially as an inhibitory modulator of channel gating over a wide [Ca^{2+}] range, dissociates from RyR2 as a result of domain unzipping of the domain switch.[13,14] Namely, the binding of CaM to RyR2 was markedly reduced in failing hearts[13] or the catecholaminergic polymorphic ventricular tachycardia (CPVT)-type knock-in mouse model (R2474S),[14] causing aberrant Ca^{2+} release and leading to HF and lethal arrhythmia. Thus, these findings suggest that aberrant unzipping of the domain switch in cardiac disorder, such as HF and CPVT, causes weakened CaM binding to the RyR2, which in turn causes leaky Ca^{2+} channels.

The CaMBD (3614–3643) of RyR1 has been reported to interact with the CaM-like domain (CaMLD: 4064–4210) of RyR1.[15] The aa 4020–4166 segment of RyR2 is homologous to the CaMLD of RyR1. Recently, Ikemoto and colleagues[16] showed that a Ca^{2+}-dependent tight interaction between the CaMBD and the CaMLD (formation of an 'activation link') activates RyR channels. More recently, they demonstrated that CaM acts as a molecular 'wedge' to inhibit excessively tight formation of the CaMBD/CaMLD activation link in endothelin-1 (ET-1)-treated neonatal cardiomyocytes and thus prevents the hypertrophy that would otherwise develop in these cells.[17] These results suggest that the excessively tight interaction between the CaMBD and the CaMLD results in the reduced CaM binding and an aberrant activation of the channel and diastolic Ca^{2+} leakage as seen in both HF and CPVT. Then, blockade of this excessively tight formation of the activation link will stabilize the channel in its closed state and will correct the channel leakage problem.

In the present study, we further investigated the underlying mechanism by which CaM dissociates from RyR2 in failing hearts and whether correction of the aberrant CaM–RyR2 interaction restores normal channel gating in failing RyR2.

2. Methods

For a detailed description, see also the expanded Materials and methods section in Supplementary material online.

2.1 Animal model

HF was induced in beagle dogs weighing 10–13 kg by continuous application of rapid ventricular pacing at 250 b.p.m. using an externally programmed miniature pacemaker (Taisho Biomed Instruments Co., Ltd) for 28 days, as described previously.[3] Dogs were deeply anaesthetized before implantation of pacemaker or removal of hearts. At the end of the study, each animal was deeply anaesthetized and euthanized with an isoflurane and intravenous injection of sodium pentobarbital (50 mg/kg). This study conformed to the Guide for the Care and Use of Laboratory Animals published by the US National Institutes of Health (NIH Publication No. 85-23, revised 1996). This study was approved by the Animal Ethics Committee of Yamaguchi University School of Medicine, and the care of the animals and the protocols used were in accordance with the guidelines laid down by the Animal Ethics Committee of Yamaguchi University School of Medicine.

2.2 Expression and purification of CaM and Gly-Ser-His-CaM

Human CaM cDNA was PCR amplified with oligonucleotide primers designated to include two restriction enzyme sites (the forward primer 5′-ACACAGGGGATCCCATATGGCTGAC-3′ and the reverse primer 5′-CAAGCTTGGCTCGAGTCACTTTGC-3′). The cDNA was inserted into a pGEX4T-1 vector. The expression vector was transformed into DH5α *Escherichia coli* (Nippongene). The strain was preincubated with Lysogeny Broth (LB) ampicillin for 16 h at 30°C followed by 2 h incubation with 10 times the volumes of LB ampicillin at 37°C.

2.3 Preparation of SR vesicles

SR vesicles were prepared from dog left ventricle (LV) muscle as previously described[3] with a slight modification. Briefly, LV homogenate was centrifuged at 5500 *g* and the resultant supernatant fraction was purified by further extensive centrifugation (12 000 *g* followed by three cycles at 143 000 *g*). The final protein concentration was 10–20 mg protein/mL.

2.4 Peptides and peptide synthesis

The following RyR2 domain peptides were used: DPc10, which harbours a CPVT-type mutation site (R2474S), and DP4090–4123, both of which have been described previously.[6,18]

DPc10 (DP2460–2495):
2460-GFCPDHKAAMVLFLD***R***VYGIEVQDFLLH
LLEVGFLP-2495
DP4090–4123:
4090-PAKDIGFNVAVLLT***N***LSEHMPNDTRLQTFLELAE-4123

Peptides were synthesized with an Applied Biosystems model 431A synthesizer using Fmoc (*N*-(9-fluorenyl)methoxycarbonyl) as the α-amino protecting group, as described previously.[19] Boldface italic letter means the position of CPVT-type mutation site.

2.5 Site-directed fluorescent labelling of the DPc10-binding site in RyR2

Specific fluorescent labelling of RyR2 was performed with the fluorescent conformational probe sulfosuccinimidyl-2-(7-azido-4-methylcoumarin-3-acetamido)ethyl-1,3′-dithiopropionate (SAED, Pierce) with DPc10 as a site-specific carrier, as described previously.[6,8]

2.6 Preparation of isolated cardiomyocytes, measurement of cell shortening, and Ca^{2+} sparks

Cardiomyocytes were isolated from the canine LV as described previously.[6] Briefly, a wedge of LV free wall was perfused with a collagenase-containing buffer solution and rod-shaped adult canine cardiomyocytes were prepared.

Ca^{2+} sparks were measured in saponin-permeabilized cardiomyocytes using Fluo-3 with a laser-scanning confocal microscope (LSM-510, Carl Zeiss).[13] Ca^{2+} spark images were obtained in the presence of the CaMKII inhibitor KN-93 (1 μmol/L). Measurements of myocyte sarcomere shortening and intracellular Ca^{2+} were performed using fura-2 AM with cells stimulated by a field electric stimulator (IonOptix, MA, USA) by 0.5 Hz. Data were analysed with SparkMaster, an automated analysis program that enables rapid and reliable spark analysis.[20]

2.7 Binding of CaM to RyR2

We assessed the binding of CaM to RyR2 using a photoreactive crosslinker, sulfosuccinimidyl-6-[4′-azido-2′-nitrophenylamino]hexanoate (Sulfo-SANPAH, Pierce), as described previously.[13] To assess direct binding ability of CaM to the RyR2 in cardiomyocytes, we added the exogenous CaM, fluorescently labelled with Alexa Fluor 633 (Molecular Probes, OR, USA), to the saponin-permeabilized cardiomyocytes. To determine the binding of endogenous CaM to the RyR2 in intact cardiomyocytes, we placed isolated cardiomyocytes on glass-based dishes, fixed with 4% paraformaldehyde in phosphate-buffered saline for 10 min, followed by immunostaining with a monoclonal mouse anti-CaM antibody and a polyclonal rabbit anti-RyR antibody.

2.8 Immunoblot analysis

Immunoblot analyses for cytological detection of CaM and RyR2 were performed using an anti-CaM antibody (Millipore, CA, USA), an anti-RyR antibody [mouse monoclonal C3-33 (Sigma) or rabbit polyclonal C-terminal Ab4963 (Sigma)], and an antibody against the RyR2 CaM-binding domain (3583–3603) (Sigma).

2.9 Measurement of the binding of exogenous CaM to RyR2 in saponin-permeabilized cardiomyocytes

Exogenous CaM was fluorescently labelled with Alexa Fluor 633 (Molecular Probes) as previously described[13] and added to saponin-permeabilized normal and failing cardiomyocytes under the same conditions described for the Ca^{2+} spark measurements. The subcellular distribution of CaM was then quantified by densitometric measurement of CaM-Alexa fluorescence.

2.10 Measurement of the binding of endogenous CaM to RyR2 in intact cardiomyocytes

Isolated cardiomyocytes were fixed with 4% paraformaldehyde and permeabilized in 0.5% Triton X-100 and 1% bovine serum albumin. Co-localization of endogenous CaM and RyR2 was then detected by immunofluorescence.

2.11 Statistics

Unpaired *t*-tests were used for statistical comparison of data obtained under two different sets of conditions. Data are expressed as means ± standard deviations (SD). A *P*-value of <0.05 was accepted as statistically significant.

3. Results

3.1 Characteristics of normal and failing heart and cardiomyocytes

After 4 weeks, pacing LV chamber size was dilated and fractional shortening was reduced (see Supplementary material online, *Table S1*). Both the width and the length of the isolated failing cardiomyocytes were larger than those of normal cardiomyocytes (see Supplementary material online, *Table S2*). The number of cells yielded from one wedge of the heart was fewer in failing hearts [$n = 4$: 155 ± 28 ($\times 10^3$), $P < 0.05$] than in normal hearts [$n = 4$: 213 ± 27 ($\times 10^3$)].

3.2 Wild-type CaM and Gly-Ser-His-CaM enhance CaMKII activity to similar extents

We tested the hypothesis (cf. Section 1) that restoring the CaM-binding stabilizes the RyR2 channel, inhibits Ca^{2+} leakage, and corrects myocyte dysfunction in failing hearts. For this purpose, we examined whether Gly-Ser-His-CaM (GSH-CaM), which was previously reported to show higher binding affinity than wild-type CaM (WT-CaM) for RyR1,[21] also shows higher binding affinity for RyR2 and thereby corrects the defects in RyR2 function in failing hearts.

There are two major pathways by which CaM regulates RyR2 channel function. The first is the inhibition of the channel by a direct interaction between CaM and RyR2, which is the main subject of the present study (cf. Section 1). The other is the activation of the channel mediated by Ca^{2+}/CaM activation of CaMKII-dependent phosphorylation of RyR2 at Ser2814.[4] In order to compare the specific effects of direct binding of GSH-CaM and WT-CaM on RyR2 channel inhibition, we inhibited CaMKII activity in cardiomyocytes with the CaMKII inhibitor KN-93 (1 μmol/L) in the present study.

We also performed the assays in the absence of the inhibitor KN-93 to determine whether there is any qualitative difference in the effects of CaM and GSH-CaM on CaMKII-mediated RyR2 activation. As shown in Supplementary material online, *Figure S1*, the concentration dependence of CaMKII activation was indistinguishable between WT-CaM and GSH-CaM. This suggests that WT-CaM and GSH-CaM may have essentially the same affinity for CaMKII.

3.3 The affinity of GSH-CaM for RyR2 is higher than that of WT-CaM

We evaluated the affinity of binding of WT-CaM and GSH-CaM to RyR2 by densitometric analysis of immunoblots of CaM cross-linked to RyR2. Regardless of whether WT-CaM or GSH-CaM was used, the anti-CaM antibody detected only RyR2 out of the many proteins in the SR, indicating that the binding of both WT-CaM and GSH-CaM is very specific to RyR2 (*Figure 1A*). The binding of either WT-CaM or GSH-CaM to RyR2 in the SR was markedly inhibited by the addition of an antibody raised against the CaMBD (3583–3603) (*Figure 1B*). This suggests that the 3583–3603 domain is indeed the major CaM/GSH-CaM-binding site of RyR2. *Figure 2A* shows that the apparent affinity of GSH-CaM for normal RyR2, which is estimated from the CaM concentration at half-maximal binding, is virtually indistinguishable from that of WT-CaM. In agreement with our previous finding,[13] the apparent affinity of CaM for RyR2 was considerably reduced in failing SR compared with normal SR, as indicated by a significant right-shift of the concentration dependence of CaM binding to RyR2 from failing heart. The apparent affinity of GSH-CaM for RyR2 from the failing heart was, however, comparable with that of WT-CaM and GSH-CaM for RyR2 from normal SR (*Figure 2A*; see also *Figure 2B*, heart failure). *Figure 2B* shows that several previously reported probes that mimic pathological conditions also considerably reduce the binding of WT-CaM, but not GSH-CaM, to RyR2 from normal SR. Thus, DPc10, which mimics the aberrant unzipping of the domain switch induced by the R2474S CPVT-type mutation,[6,22] and DP4090–4123,[18] which mimics the CPVT-linked defective inter-domain interaction between the I domain (3772–4610)[23] and its

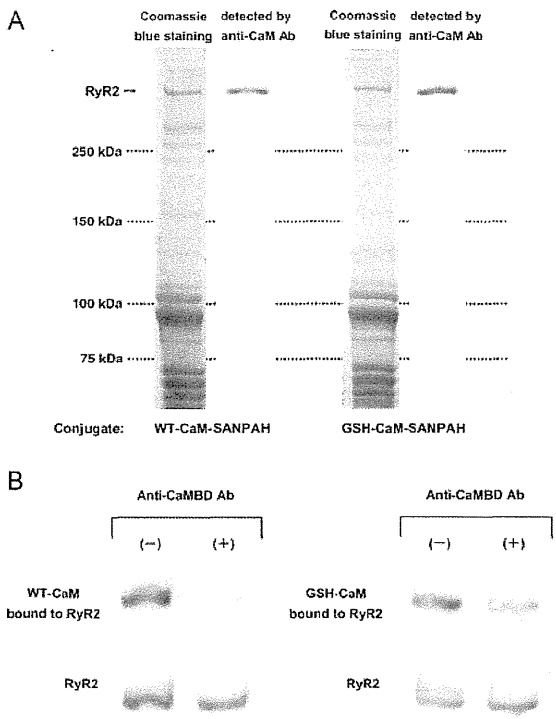

Figure 1 Cross-linking of CaM or GSH-CaM to the ryanodine receptor (RyR2). (*A*) Representative immunoblot of CaM or GSH-CaM cross-linked to RyR2. Note that the anti-CaM (or GSH-CaM) antibody detected only RyR2 among the many proteins in the SR. (*B*) Effect of the antibody against the CaM-binding domain (3583–3603; anti-CaMBD antibody) of RyR2 on CaM (or GSH-CaM) binding to RyR2.

putative partner domain, significantly reduced the binding of WT-CaM but only slightly reduced the binding of GSH-CaM to RyR2 (*Figure 2B*).

3.4 Binding of CaM but not GSH-CaM to RyR2 is inhibited by DPc10 and DP4090–4123 in isolated cardiomyocytes

To assess whether the high-affinity binding of GSH-CaM to RyR2 under pathological conditions that we observed in the isolated SR is also preserved in cardiomyocytes, we examined the effect of DP4090–4123 or DPc10 on the binding affinities of CaM and GSH-CaM for RyR2 in cells. We evaluated the binding of Alexa-labelled WT-CaM or GSH-CaM to subcellular fractions of saponin-permeabilized cardiomyocytes (see Supplementary material online, *Figure S2*). Both WT-CaM-Alexa and GSH-CaM-Alexa co-localized with the anti-RyR2 immunostaining, suggesting that exogenous WT-CaM and GSH-CaM introduced into cardiomyocytes both bind to the RyR2 (see Supplementary material online, *Figure S2*). When we plotted the intensity of the Alexa fluorescence along the sarcomeres (see Section 2) as a function of the concentration of the introduced CaM-Alexa or GSH-CaM-Alexa in normal myocytes (Normal), the concentration dependence of GSH-CaM binding was slightly shifted towards the lower concentrations below 100 nmol/L and unchanged above 100 nmol/L relative to the dependence of WT-CaM binding (*Figure 3*). In the cardiomyocytes treated with either DPc10 or DP4090–4123, however, the concentration dependence of WT-CaM binding was greatly shifted towards higher concentrations, while the binding affinity of GSH-CaM appeared unchanged. These data suggest that defective inter-domain interaction (domain unzipping) of either the domain switch or the near C-terminal region [the CaMLD (4020–4166) and its partner domain] commonly reduces the binding of CaM to RyR2, while GSH-CaM can maintain normal binding to RyR2 even in the presence of either peptide. GSH-CaM, but not WT-CaM, bound normally to RyR2 in failing cardiomyocytes. These results are consistent with the data for CaM-SANPAH binding to RyR2 in the SR vesicles (*Figure 2*).

3.5 Increased CaM binding affinity corrects elevated Ca^{2+} spark frequency in saponin-permeabilized failing cardiomyocytes

To examine whether correction of the defective interaction between CaM and RyR2 inhibits spontaneous Ca^{2+} release events, we measured the frequency of Ca^{2+} sparks in saponin-permeabilized cardiomyocytes (*Figure 4*). Both DPc10 and DP4090–4123 increased the Ca^{2+} spark frequency (SpF) in normal cardiomyocytes. Exogenous GSH-CaM, but not WT-CaM, blocked the increases in SpF induced by both peptides. The baseline Ca^{2+} SpF was significantly increased in failing cardiomyocytes. The addition of GSH-CaM, but not WT-CaM, blocked the increase in SpF. As shown in *Figure 4B*, both the full width at half-maximum (FWHM) and full duration at half-maximum (FDHM) increased under all pathological conditions (cardiomyocytes from failing hearts or normal myocytes treated with DPc10 or DP4090–4123), and GSH-CaM corrected both parameters to noticeable extents than did WT-CaM. In contrast to the greater spark frequencies observed under pathological conditions, the Ca^{2+} spark amplitudes were lower in both peptide-treated normal cardiomyocytes and failing cardiomyocytes, and GSH-CaM increased the Ca^{2+} spark amplitude to a greater extent than did WT-CaM.

As shown in the bottom panel of *Figure 4B*, both peptides increased the SpF and decreased the SR Ca^{2+} content. GSH-CaM, but not WT-CaM, prevented the peptide-induced increase in SpF and decrease in SR Ca^{2+} content. Baseline SpF was increased and SR Ca^{2+} content decreased in failing cardiomyocytes, and both were restored to normal levels by GSH-CaM but not by WT-CaM.

3.6 GSH-CaM corrects defective Ca^{2+} transient and cell shortening in intact ('non-permeabilized') failing cardiomyocytes

3.6.1 Incorporation of WT-CaM or GSH-CaM into intact cardiomyocytes and effects of WT-CaM and GSH-CaM on peptide-treated normal cardiomyocytes and failing cardiomyocytes

Incorporation of either WT-CaM or GSH-CaM into intact cardiomyocytes was successfully achieved by the use of a protein delivery kit (see Supplementary material online, Expanded Materials and Methods). The intracellular concentrations of GSH-CaM and CaM were 127 ± 38 nmol/L ($n = 6$ cells) and 131 ± 55 nmol/L ($n = 7$ cells), respectively (difference: statistically insignificant). As shown in Supplementary material online, *Figure S3*, CaM was detected along the sarcomeres by immunostaining and co-localized with RyR2.

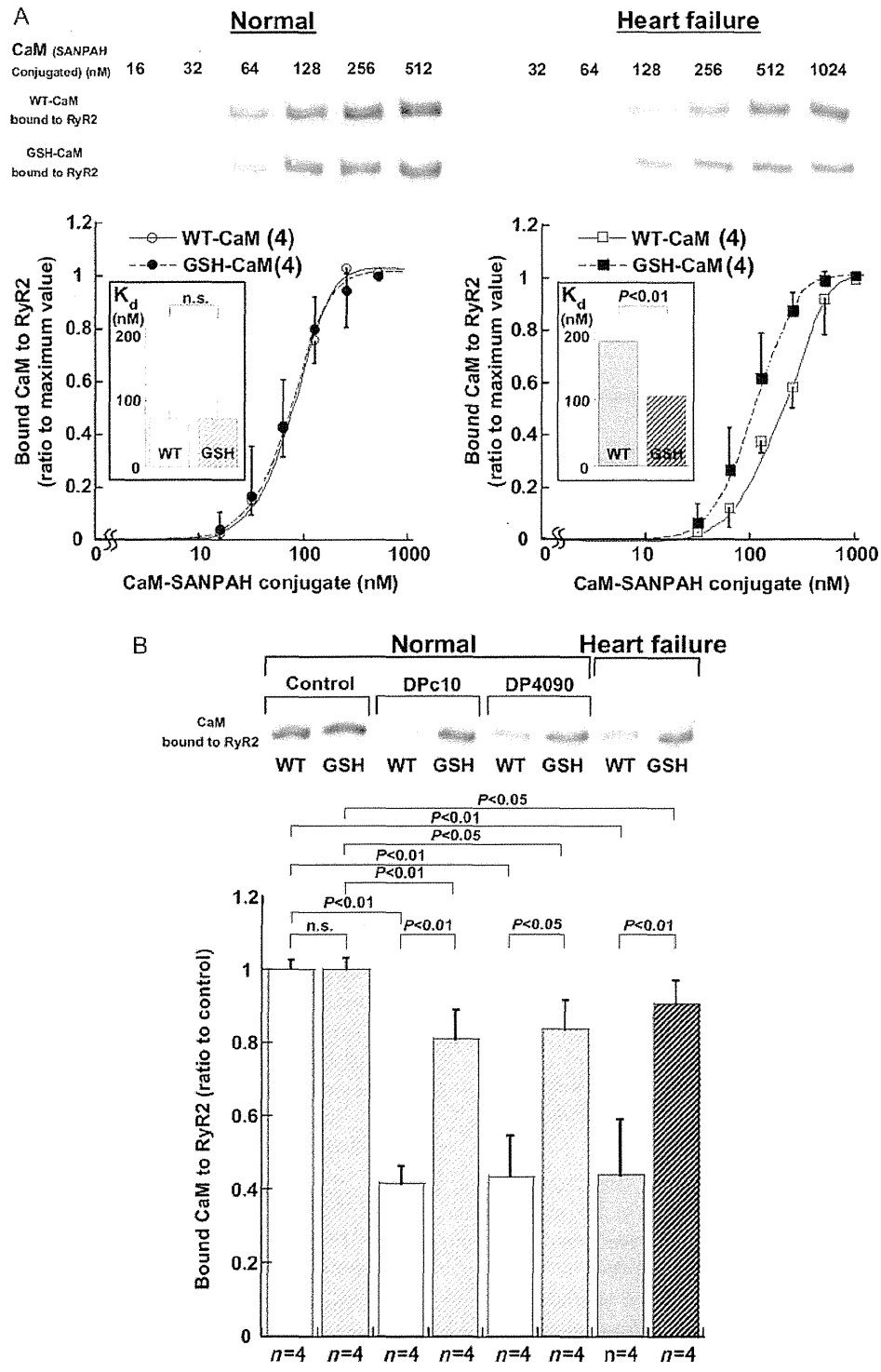

Figure 2 (*A*) CaM (or GSH-CaM) concentration dependence of the binding of CaM to normal RyR2 (top) and the summarized data (bottom). The immunoblot density of the CaM cross-linked to RyR2 was determined at various concentrations of CaM (or GSH-CaM)-SANPAH as indicated and expressed as the ratio to the maximum value obtained at 1 μmol/L CaM (or GSH-CaM). Each datum point per concentration represents mean ± SD of four SR preparations from four hearts, and the sigmoid concentration-dependent relationships for CaM binding was fitted by an equation: $y = aK^n x^n/(1 + K^n x^n)$, and the EC_{50} values were calculated as $1/K$. (Inset) Comparison of EC_{50}. Paired *t*-test was employed to determine the statistical significance of EC_{50}. The numerical value in the parenthesis means the number of concentration-dependent relationships for CaM binding. (*B*) Cross-linking of CaM or GSH-CaM (128 nmol/L) to RyR2 in DPc10 (30 μmol/L)- or DP4090–4123 (30 μmol/L)-treated SR vesicles from normal and failing hearts. Representative immunoblots of CaM bound to RyR2 (top) and summarized data (bottom) are shown. The immunoblot density of CaM cross-linked to RyR2 was measured and expressed as the ratio to the control. Data represent the means ± SD obtained from four SR preparations.

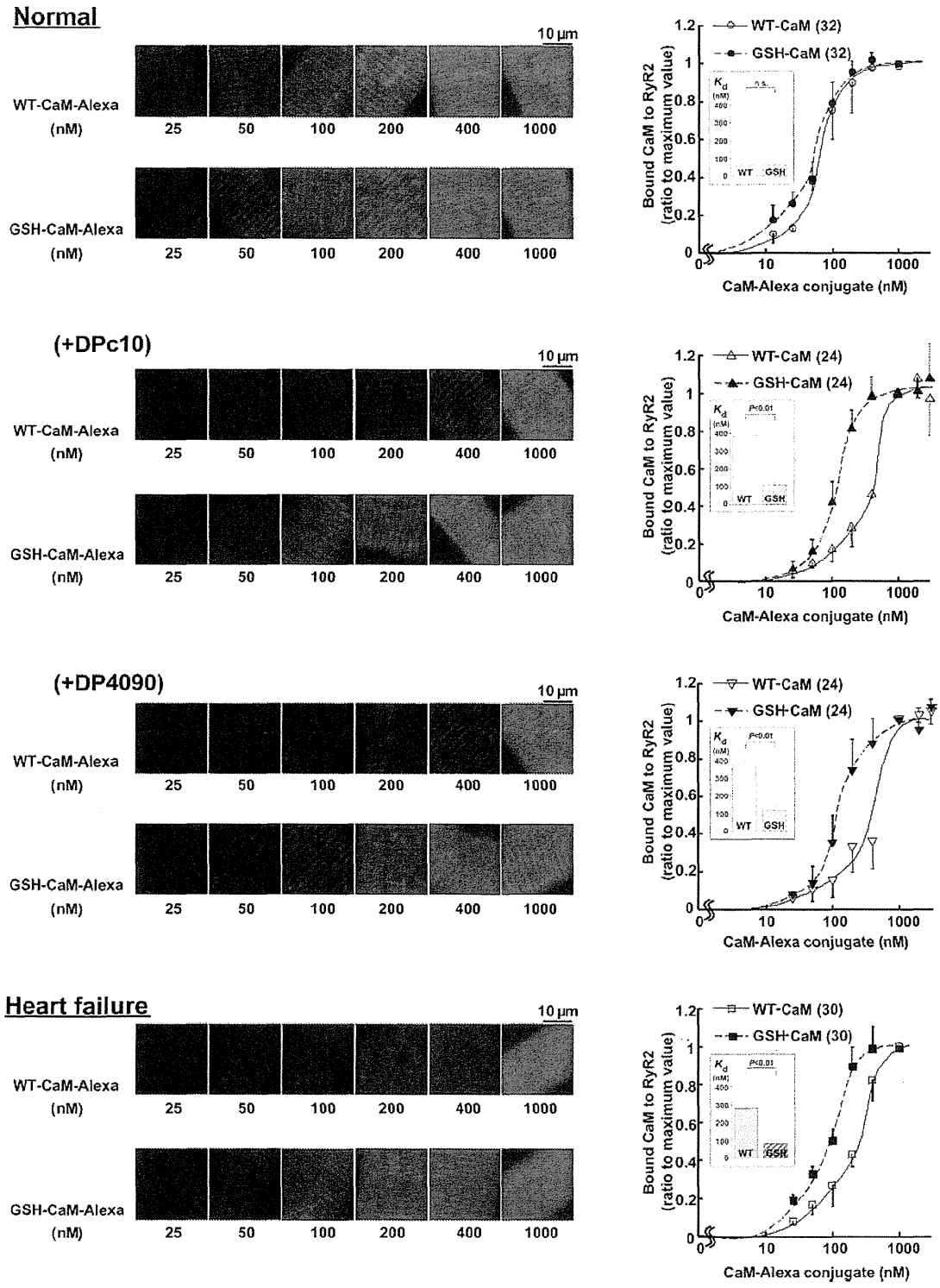

Figure 3 The binding characteristics of exogenously introduced CaM in saponin-permeabilized cardiomyocytes. Delivery of various concentrations of CaM-Alexa or GSH-CaM-Alexa (left panel) and the summarized data (right panel) in normal cardiomyocytes and failing cardiomyocytes treated with RyR2 domain peptides (DPc10, 30 μmol/L, or DP4090–4123, 30 μmol/L). Either WT-CaM-Alexa or GSH-CaM-Alexa fluorescence was measured and expressed as the ratio to its maximum value. Each datum point per concentration represents mean ± SD of 8–10 cells from three to four hearts, and the sigmoid concentration-dependent relationships for CaM binding was fitted by an equation: $y = aK^n x^n/(1 + K^n x^n)$, and the EC_{50} values were calculated as 1/K. (Inset) Comparison of EC_{50}. Paired *t*-test was employed to determine the statistical significance of EC_{50}. The numerical value in the parenthesis means the number of concentration-dependent relationships for CaM binding.

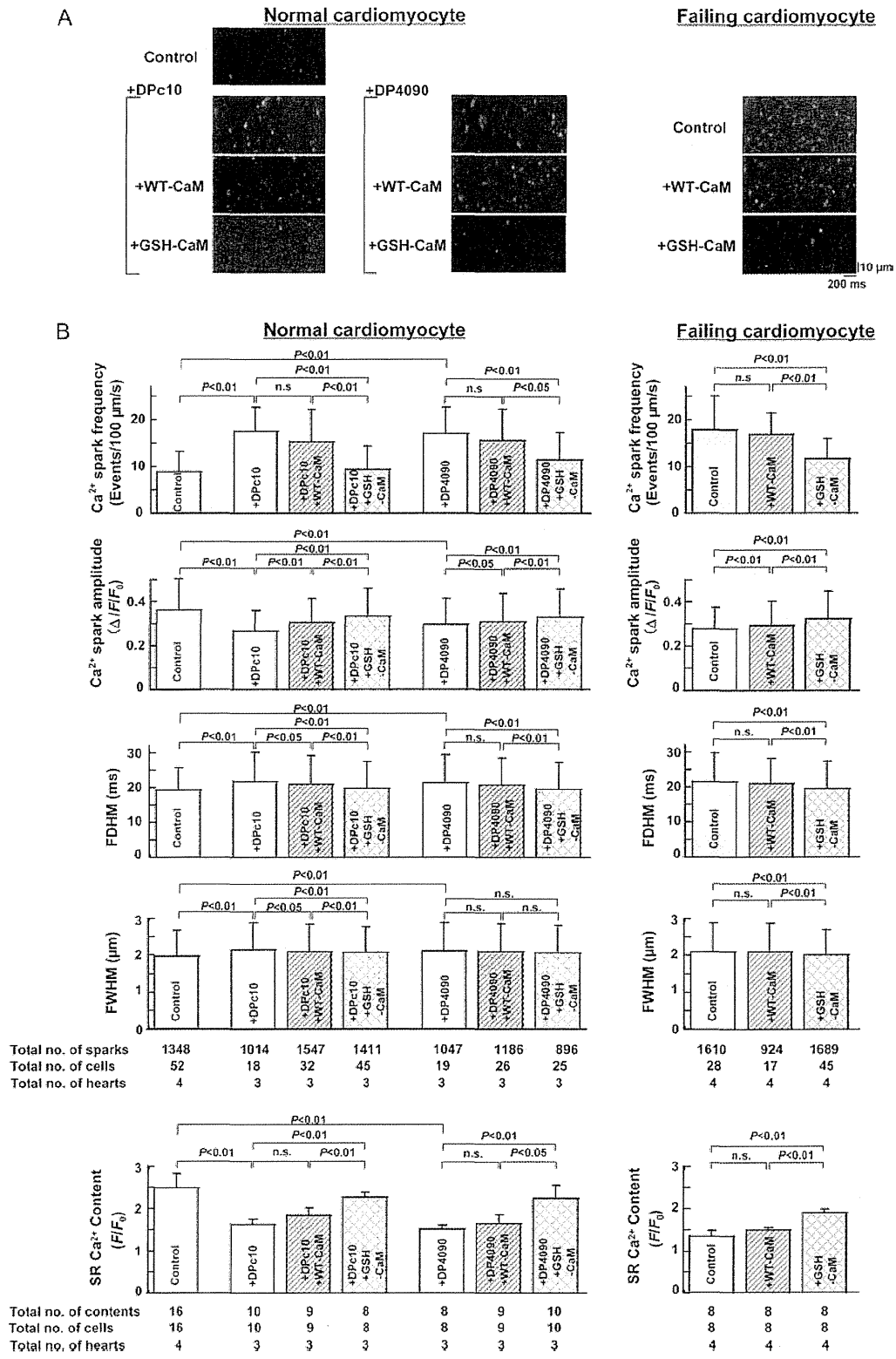

Figure 4 Effect of WT-CAM (or GSH-CaM) (200 nmol/L) on Ca^{2+} SpF and SR Ca^{2+} content in (saponin-permeabilized) normal cardiomyocytes and failing cardiomyocytes treated with RyR2 domain peptides (DPc10, 30 μmol/L, or DP4090–4123, 30 μmol/L). SR Ca^{2+} content was measured by adding 10 mmol/L caffeine. Ca^{2+} spark images were obtained in the presence of the CaMKII inhibitor KN-93 (1 μmol/L). (*A*) Representative images of Ca^{2+} sparks. (*B*) Summarized data of the FDHM, FWHM, Ca^{2+} spark amplitude, Ca^{2+} SpF, and SR Ca^{2+} content. Data represent the means ± SD of 8–32 cells from each of three to four hearts.

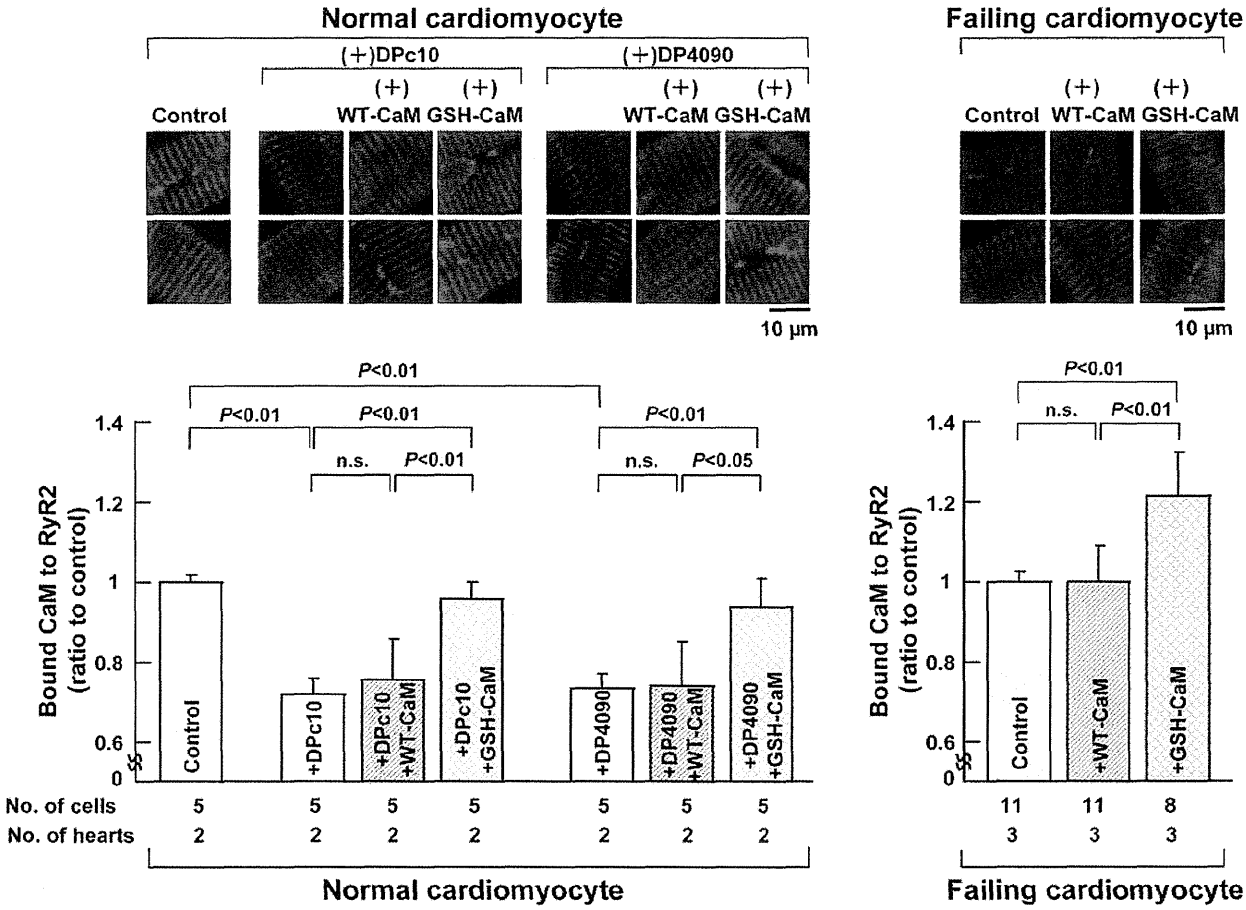

Figure 5 Effect of incorporation of WT-CaM or GSH-CaM on the binding of CaM to RyR2. Representative images of the binding of CaM to RyR2 (top) and the summarized data (bottom) are shown. Data represent means ± SD of 5–11 cells from each of two to three hearts.

Both DPc10 and DP4090–4123 decreased the binding of endogenous CaM to RyR2. GSH-CaM, but not WT-CaM, restored normal binding to RyR2; a similar pattern was seen in failing cardiomyocytes, in which CaM-GSH, but not WT-CaM, restored CaM binding to RyR2 (*Figure 5*).

As shown in Supplementary material online, *Figure S4*, Ca SpF was increased and SR Ca^{2+} content was reduced in intact (non-permeabilized) failing cardiomyocytes. Importantly, the incorporation of GSH-CaM (by protein delivery kit), but not WT-CaM, restored normal levels in the intact non-permeabilized cardiomyocytes, as in the case of permeabilized myocytes. KN93 was without an effect on Ca^{2+} SpF and SR Ca^{2+} content in both intact (non-permeabilized) normal and failing cardiomyocytes (see Supplementary material online, *Figure S5*).

3.6.2 Effect of WT-CaM or GSH-CaM on Ca^{2+} transient and cell shortening in normal and failing cardiomyocytes

Figure 6B summarizes the characteristics of both Ca^{2+} transient and cell shortening in normal and failing cardiomyocytes. As shown, both Ca^{2+} transient and cell shortening were reduced in both DPc10- or DP4090–4123-treated normal cardiomyocytes and failing cardiomyocytes (*Figure 6A*). Incorporation of GSH-CaM but not WT-CaM improved both cell shortening and Ca^{2+} transient in DPc10- or DP4090–4123-treated normal cardiomyocytes and failing cardiomyocytes. KN93 was without the effect on Ca^{2+} transient and cell shortening in both intact (non-permeabilized) normal and failing cardiomyocytes (see Supplementary material online, *Figure S6*).

To investigate the kinetic response of the contractile proteins to changes in $[Ca^{2+}]$, we plotted per cent cell shortening as a function of Ca^{2+} transient (see Supplementary material online, *Figure S7*). Although the area of the cell shortening-Ca^{2+} transient loop was reduced in DPc10- or DP4090–4123-added normal cardiomyocytes and failing cardiomyocytes, the slope during the deceleration phase of Ca^{2+} transient was virtually unchanged among all groups. This suggests that the dynamic Ca^{2+} sensitivity did not change by domain unzipping and subsequent Ca^{2+} leakage. GSH-CaM, but not WT-CaM, normally restored the area of the loop in DPc10- or DP4090–4123-added normal cardiomyocytes and failing cardiomyocytes.

4. Discussion

Accumulated evidence concerning the pathogenic mechanism of HF suggests that abnormal intracellular Ca^{2+} handling leads to cardiac dysfunction and lethal arrhythmia.[24]

The most important aspect of the present study is the finding that correction of the reduced CaM binding in the 'destabilized' RyR2 to a

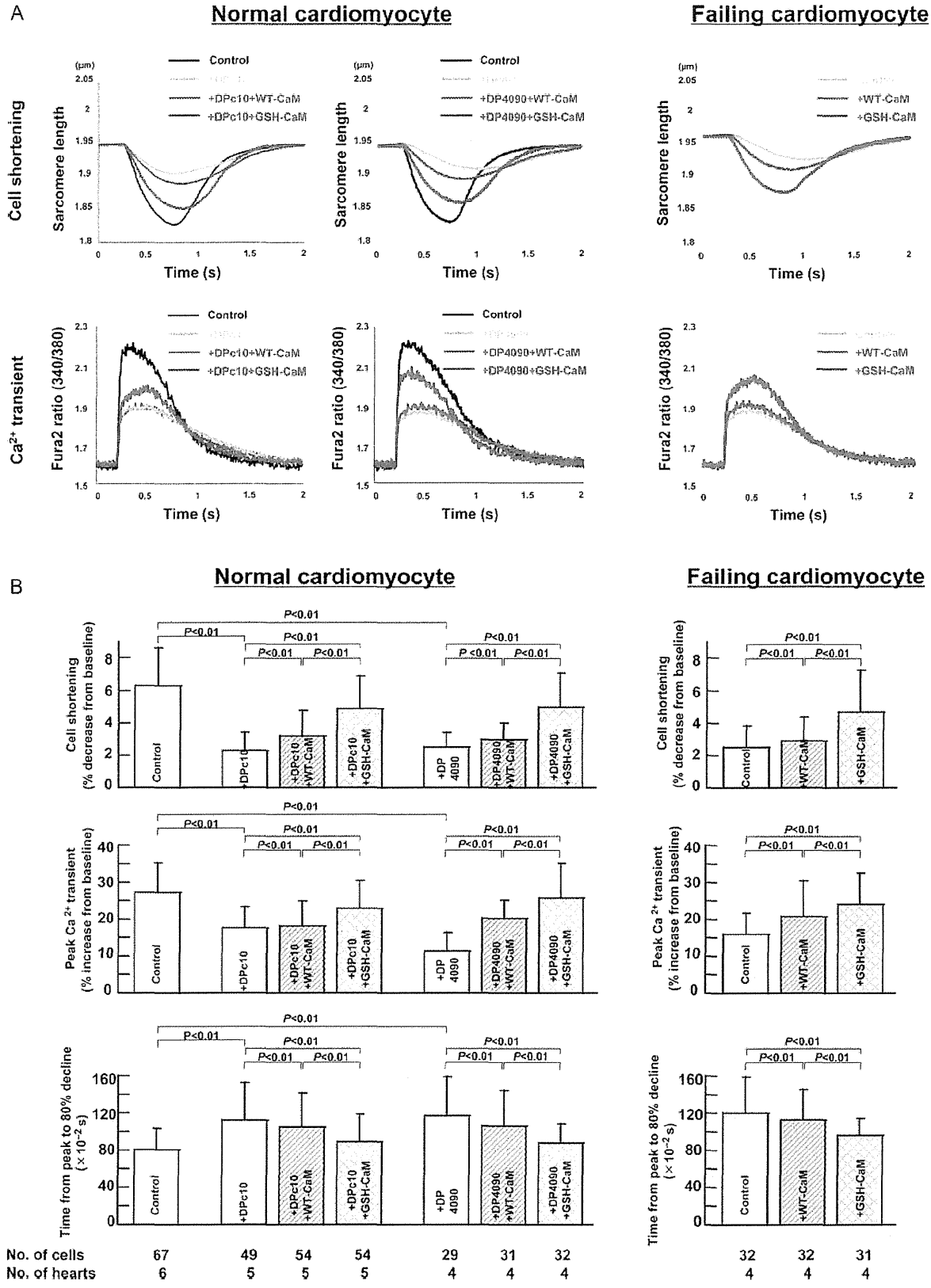

Figure 6 Effect of CaM or GSH-CaM on Ca^{2+} transient and cell shortening in normal and failing cardiomyocytes. (*A*) Representative tracings of Ca^{2+} transient and cell shortening in normal and failing cardiomyocytes. (*B*) The characteristics of cell shortening and Ca^{2+} transient in normal and failing cardiomyocytes treated with RyR2 domain peptides (DPc10, 30 μmol/L, or DP4090–4123, 30 μmol/L).

normal level restores normal channel gating and improves contractile function in failing hearts (see Supplementary material online, *Figure S8*). This indicates that increased binding of CaM serves as a 'natural therapeutic agent,' a hypothesis supported by the following evidence. GSH-CaM, which shows higher binding affinity than WT-CaM for RyR2, supported a normal level of CaM binding to RyR2 when added to CPVT-type defective RyR2 experimentally produced by DPc10 or DP4090–4123, where the binding affinity of WT-CaM is much reduced. Consequently, the increased CaM binding prevented diastolic Ca^{2+} leakage as indicated by the reduced frequency of spontaneous Ca^{2+} sparks. Similarly, the binding of GSH-CaM to RyR2 from failing cardiomyocytes restored normal spontaneous Ca^{2+} SpF, Ca^{2+} transient, and cell shortening.

The following important question then arises: what is the mechanism by which the RyR2-bound CaM controls RyR2 channel function? It has been postulated that the CaMLD/CaMBD interaction activates the Ca^{2+} channel, while competitive binding of CaM to the CaMBD suppresses channel activation and stabilizes the closed state of the channel (cf. Section 1).[16] Under pathological conditions such as HF and CPVT, the CaMLD/CaMBD interaction becomes excessively tight, which overcomes the intrinsic affinity CaM for its binding to the CaMBD. According to this scheme, increasing the CaM binding affinity over the intrinsic level restores the ability of CaM to 'wedge' and disrupts the excessively tight channel activation interaction between the CaMLD and the CaMBD. In the present study, the introduction of GSH-CaM, which has a significantly higher affinity than WT-CaM for RyR2, permitted us to demonstrate that this previously postulated mechanism in fact operates. Importantly, we have further shown that dantrolene, which corrects defective unzipping, restored a normal level of binding of WT-CaM and normal RyR2 function in these disease models.[13,14] These findings clearly indicate that the formation of an excessively tight CaMLD/CaMBD interaction, which causes aberrant channel activation, is mediated by unzipping (perhaps sustained unzipping) of the domain switch.

Ikemoto and colleagues[17] recently showed that hypertrophic stimulus of neonatal cardiomyocytes with ET-1 induced dissociation of CaM from RyR2; this leads to a sequence of intracellular events including increased frequency of spontaneous Ca^{2+} transients and translocation of CaM, CaMKII, and N-FAT to the nucleus. They further demonstrated that an anti-CaMBD antibody, used as a 'molecular wedge' to disrupt the CaMBD/CaMLD interaction, prevented all of these ET-1-induced pathological intracellular events and consequently the development of hypertrophy.[25] These data support the hypothesis that aberrant formation of the channel-activating interaction between the CaMBD and the CaMLD of RyR2 is an early key event leading to the development of hypertrophy in this cell model.

Thus, our recent and present findings suggest that unzipping of the domain switch and zipping of the CaMBD/CaMLD pair are coupled for the channel opening. According to George *et al.*,[23] channel function is regulated by the interaction between RyR cytoplasmic and transmembrane domains via amino acids residues 3722–4610 (designated as I-domain), and leaky Ca^{2+} channels are characterized by unstable interactions between the I domain and the transmembrane channel domain. The present finding that DP4090–4123, a peptide corresponding to a part of the I-domain, activated the channel presumably by interfering with a tight interaction of the I-domain with the channel domain, causing their unzipping. Summarizing the accumulated pieces of information, we propose a general hypothesis that in the systolic phase of normal channels, unzipping of (A) the domain switch (the N-terminal domain/central domain pair), zipping (formation of a tight link) of (B) the CaMBD/CaMLD pair, and unzipping of (C) the I-domain/channel domain pair are conformationally coupled in an allosteric manner to activate the channel. In the diastolic phase of normal operation, reversed conformational changes take place in these three interacting pairs, again in a tightly coupled manner. In disease models, and peptide-treated mimicries of the pathological state, destabilization of the zipped state of regions A and C and formation of a tighter link in the region B take place again in a conformationally coupled manner in the diastolic state, causing erroneous channel activation and diastolic Ca^{2+} leakage. This scheme of conformational coupling suggests the possibility that correcting the problem in any of these three regions (A, B, and C) might correct the defective conformational state in the other regions. However, according to our preliminary data (not shown), the addition of GSH-CaM to SR from failing hearts or SR treated with DPc10, which restored normal CaM binding and normal channel closing, could not fully restore the normal zipped state of the domain switch. This suggests that in pathological conditions, the conformational coupling from the region B to the region A is loose or incomplete presumably owing to a sustained, or chronic, unzipped state of the domain switch, which can be restored to normal zipped state only by the agents such as dantrolene and K201 that are directed to the domain switch.

Although the pacing-induced HF model is widely recognized as a representative model of human HF because of the structural and functional similarity, whether we can extrapolate the present findings to other HF (e.g. post-myocardial infarction, ischaemic cardiomyopathy, hypertensive heart disease, etc.) must wait for future studies.

In conclusion, the defective inter-domain interaction between the N-terminal domain and the central domain within RyR2, coupled with a second defective inter-domain interaction between the CaMBD and the CaMLD, plays a key role in the pathogenic mechanism by which the channel is destabilized. The reduced binding of CaM to RyR2 caused by the defective inter-domain interactions predisposes failing hearts to aberrant Ca^{2+} release and lethal arrhythmia. Correction of the reduced CaM binding to the failing RyR2 can stabilize the channel function in the diseased hearts.

Supplementary material

Supplementary material is available at *Cardiovascular Research* online.

Conflict of interest: none declared.

Funding

This work was supported by grants-in-aid for scientific research from The Ministry of Education in Japan (grant nos 22659154 and 23390215 to M.Y., 23591082 to T.Y., and 23592256 to S.K.) and grant from the National Heart, Lung and Blood Institutes (HL072841 to N.I.).

References

1. Bers DM. Macromolecular complexes regulating cardiac ryanodine receptor function. *J Mol Cell Cardiol* 2004;**37**:417–429.
2. Marx SO, Reiken S, Hisamatsu Y, Jayaraman T, Burkhoff D, Rosemblit N *et al.* PKA phosphorylation dissociates FKBP12.6 from the calcium release channel (ryanodine receptor): defective regulation in failing hearts. *Cell* 2000;**101**:365–376.

3. Yano M, Ono K, Ohkusa T, Suetsugu M, Kohno M, Hisaoka T *et al.* Altered stoichiometry of FKBP12.6 versus ryanodine receptor as a cause of abnormal Ca^{2+} leak through ryanodine receptor in heart failure. *Circulation* 2000;**102**:2131–2136.
4. Guo T, Zhang T, Mestril R, Bers DM. Ca^{2+}/calmodulin-dependent protein kinase II phosphorylation of ryanodine receptor does affect calcium sparks in mouse ventricular myocytes. *Circ Res* 2006;**99**:398–406.
5. Maier LS, Zhang T, Chen L, DeSantiago J, Brown JH, Bers DM. Transgenic CaMKIIdeltaC overexpression uniquely alters cardiac myocyte Ca^{2+} handling: reduced SR Ca^{2+} load and activated SR Ca^{2+} release. *Circ Res* 2003;**92**:904–911.
6. Oda T, Yano M, Yamamoto T, Tokuhisa T, Okuda S, Doi M *et al.* Defective regulation of interdomain interactions within the ryanodine receptor plays a key role in the pathogenesis of heart failure. *Circulation* 2005;**111**:3400–3410.
7. Yano M, Okuda S, Oda T, Tokuhisa T, Tateishi H, Mochizuki M *et al.* Correction of defective interdomain interaction within ryanodine receptor by antioxidant is a new therapeutic strategy against heart failure. *Circulation* 2005;**112**:3633–3643.
8. Yamamoto T, Yano M, Xu X, Uchinoumi H, Tateishi H, Mochizuki M *et al.* Identification of target domains of the cardiac ryanodine receptor to correct channel disorder in failing hearts. *Circulation* 2008;**117**:762–772.
9. Kobayashi S, Yano M, Suetomi T, Ono M, Tateishi H, Mochizuki M *et al.* Dantrolene, a therapeutic agent for malignant hyperthermia, markedly improves the function of failing cardiomyocytes by stabilizing interdomain interactions within the ryanodine receptor. *J Am Coll Cardiol* 2009;**53**:1993–2005.
10. Rodney GG, Williams BY, Strasburg GM, Beckingham K, Hamilton SL. Regulation of RyR1 activity by Ca^{2+} and calmodulin. *Biochemistry* 2000;**39**:7807–7812.
11. Yamaguchi N, Xu L, Pasek DA, Evans KE, Meissner G. Molecular basis of calmodulin binding to cardiac muscle Ca^{2+} release channel (ryanodine receptor). *J Biol Chem* 2003;**278**:23480–23486.
12. Yamaguchi N, Takahashi N, Xu L, Smithies O, Meissner G. Early cardiac hypertrophy in mice with impaired calmodulin regulation of cardiac muscle Ca release channel. *J Clin Invest* 2007;**117**:1344–1353.
13. Ono M, Yano M, Hino A, Suetomi T, Xu X, Susa T *et al.* Dissociation of calmodulin from cardiac ryanodine receptor causes aberrant Ca^{2+} release in heart failure. *Cardiovasc Res* 2010;**87**:609–617.
14. Xu X, Yano M, Uchinoumi H, Hino A, Suetomi T, Ono M *et al.* Defective calmodulin binding to the cardiac ryanodine receptor plays a key role in CPVT-associated channel dysfunction. *Biochem Biophys Res Commun* 2010;**394**:660–666.
15. Xiong L, Zhang JZ, He R, Hamilton SL. A Ca^{2+}-binding domain in RyR1 that interacts with the calmodulin binding site and modulates channel activity. *Biophys J* 2006;**90**:173–182.
16. Gangopadhyay JP, Ikemoto N. Interaction of the Lys(3614)-Asn(3643) calmodulin-binding domain with the Cys(4114)-Asn(4142) region of the type 1 ryanodine receptor is involved in the mechanism of Ca^{2+}/agonist-induced channel activation. *Biochem J* 2008;**411**:415–423.
17. Gangopadhyay JP, Ikemoto N. Aberrant interaction of calmodulin with the ryanodine receptor develops hypertrophy in the neonatal cardiomyocyte. *Biochem J* 2011;**438**:379–387.
18. Tateishi H, Yano M, Mochizuki M, Suetomi T, Ono M, Xu X *et al.* Defective domain–domain interactions within the ryanodine receptor as a critical cause of diastolic Ca^{2+} leak in failing hearts. *Cardiovasc Res* 2009;**81**:536–545.
19. Yamamoto T, Ikemoto N. Peptide probe study of the critical regulatory domain of the cardiac ryanodine receptor. *Biochem Biophys Res Commun* 2002;**291**:1102–1108.
20. Picht E, Zima AV, Blatter LA, Bers DM. SparkMaster: automated calcium spark analysis with ImageJ. *Am J Physiol* 2007;**293**:c1073–c1081.
21. Moore CP, Rodney G, Zhang JZ, Santacruz-Toloza L, Strasburg G, Hamilton SL. Apocalmodulin and Ca^{2+} calmodulin bind to the same region on the skeletal muscle Ca^{2+} release channel. *Biochemistry* 1999;**38**:8532–8537.
22. Uchinoumi H, Yano M, Suetomi T, Ono M, Xu X, Tateishi H *et al.* Catecholaminergic polymorphic ventricular tachycardia is caused by mutation-linked defective conformational regulation of the ryanodine receptor. *Circ Res* 2010;**106**:1413–1424.
23. George CH, Jundi H, Thomas NL, Scoote M, Walters N, Williams AJ *et al.* Ryanodine receptor regulation by intramolecular interaction between cytoplasmic and transmembrane domains. *Mol Biol Cell* 2004;**15**:2627–2638.
24. Yano M, Ikeda Y, Matsuzaki M. Altered intracellular Ca^{2+} handling in heart failure. *J Clin Invest* 2005;**115**:556–564.
25. Gangopadhyay JP, Ikemoto N. Intracellular translocation of calmodulin and Ca^{2+}/calmodulin-dependent protein kinase II during the development of hypertrophy in neonatal cardiomyocytes. *Biochem Biophys Res Commun* 2010;**396**:515–521.

Basic Science and Experimental Studies

Striking Volume Intolerance Is Induced by Mimicking Arterial Baroreflex Failure in Normal Left Ventricular Function

KOUTA FUNAKOSHI, MD,[1] KAZUYA HOSOKAWA, PhD,[1] TAKUYA KISHI, PhD,[2] TOMOMI IDE, PhD,[1] AND KENJI SUNAGAWA, PhD[1]

Fukuoka, Japan

ABSTRACT

Background: Patients with heart failure and preserved ejection fraction (HFpEF) are supersensitive to volume overload, and a striking increase in left atrial pressure (LAP) often occurs transiently and is rapidly resolved by intravascular volume reduction. The arterial baroreflex is a powerful regulator of intravascular stressed blood volume. We examined whether arterial baroreflex failure (FAIL) mimicked by constant carotid sinus pressure (CSP) causes a striking increase in LAP and systemic arterial pressure (AP) by volume loading in rats with normal left ventricular (LV) function.

Methods and Results: In anesthetized Sprague-Dawley rats, we isolated bilateral carotid sinuses and controlled CSP by a servo-controlled piston pump. We mimicked the normal arterial baroreflex by matching CSP to instantaneous AP and FAIL by maintaining CSP at a constant value regardless of AP. We infused dextran stepwise (infused volume [Vi]) until LAP reached 15 mm Hg and obtained the LAP-Vi relationship. We estimated the critical Vi as the Vi at which LAP reached 20 mm Hg. In FAIL, critical Vi decreased markedly from 19.4 ± 1.6 mL/kg to 15.6 ± 1.6 mL/kg ($P < .01$), whereas AP at the critical Vi increased (194 ± 6 mm Hg vs 163 ± 6 mm Hg; $P < .01$). We demonstrated that an artificial arterial baroreflex system we recently developed could fully restore the physiologic volume intolerance in the absence of native arterial baroreflex.

Conclusions: Arterial baroreflex failure induces striking volume intolerance in the absence of LV dysfunction and may play an important role in the pathogenesis of acute heart failure, especially in states of HFpEF. (*J Cardiac Fail 2014;20:53–59*)

Key Words: Heart failure, arterial baroreflex, volume intolerance.

A subgroup of patients with acute decompensated heart failure often experience sudden onset of pulmonary edema with a striking increase in left atrial pressure (LAP). Epidemiologic studies revealed that approximately one-half of these patients have preserved left ventricular (LV) ejection fraction (LVEF), a condition known as heart failure with preserved LVEF (HFpEF).[1–4] These patients have marked hypertension at admission[1–4] and rapid onset of symptoms,[5] though they have few symptoms in the chronic phase.[6] Moreover, the striking increase in LAP may occur only transiently and is rapidly resolved with mild volume reduction by diuresis.[7] In other words, patients with acute decompensated heart failure are supersensitive to volume overload and have volume intolerance regardless of LVEF.

Many studies have shown that patients with HFpEF have structural and functional changes consistent with concentric remodeling and dominant abnormalities in LV diastolic function, whereas patients with reduced LVEF have eccentric remodeling and LV systolic dysfunction.[8–15] The most common causes of HFpEF include chronic hypertension and age-associated cardiovascular changes.[7] However, therapies with unequivocal benefits for heart failure with

From the [1]Department of Cardiovascular Medicine, Kyushu University Graduate School of Medical Sciences, Fukuoka, Japan and [2]Department of Advanced Therapeutics for Cardiovascular Diseases, Kyushu University Graduate School of Medical Sciences, Fukuoka, Japan.

Manuscript received August 14, 2013; revised manuscript received November 15, 2013; revised manuscript accepted November 19, 2013.

Reprint requests: Takuya Kishi, PhD, Department of Advanced Therapeutics for Cardiovascular Diseases, Kyushu University Graduate School of Medical Sciences, 3-1-1 Maidashi, Higashi-ku, Fukuoka 812-8582, Japan. Tel: +81-92-642-5360; Fax: +81-92-642-5374. E-mail: tkishi@cardiol.med.kyushu-u.ac.jp

Funding: Health and Labour Sciences Research Grant for Research on Medical Devices for Improving Impaired QOL and Health and Labour Sciences Research Grant for Clinical Research from the Ministry of Health, Labor, and Welfare of Japan and a Grant-in-Aid for Scientific Research (S) (18100006) from the Japan Society for the Promotion of Science.

See page 58 for disclosure information.

1071-9164/$ - see front matter

http://dx.doi.org/10.1016/j.cardfail.2013.11.007